nature biomedical engineering

ARTICLES

PUBLISHED: 6 MARCH 2017 | VOLUME: 1 | ARTICLE NUMBER: 0037

Cross-circulation for extracorporeal support and recovery of the lung

John D. O'Neill[1†], Brandon A. Guenthart[1,2†], Jinho Kim[1], Scott Chicotka[2], Dawn Queen[1], Kenmond Fung[3], Charles Marboe[4], Alexander Romanov[5], Sarah X. L. Huang[6,7], Ya-Wen Chen[6,7], Hans-Willem Snoeck[6,7,8,9], Matthew Bacchetta[2*] and Gordana Vunjak-Novakovic[1,7*]

The shortage of transplantable donor organs has profound consequences, especially for patients with end-stage lung disease, for which transplantation remains the only definitive treatment. Although advances in *ex vivo* lung perfusion have enabled the evaluation and reconditioning of marginally unacceptable donor lungs, clinical use of the technique is limited to ~6 h. Extending the duration of extracorporeal organ support from hours to days would enable longer recovery and recipient-specific manipulations of the donor lung, with the goal of expanding the donor organ pool and improving long-term outcomes. By using a clinically relevant swine model, here we report the development of a cross-circulation platform wherein recipient support enabled 36 h of normothermic perfusion that maintained healthy lungs and allowed for the recovery of injured lungs. Extended support enabled multiscale therapeutic interventions in all extracorporeal lungs. Lungs exceeded transplantation criteria, and recipients tolerated cross-circulation with no significant changes in physiologic parameters throughout 36 h of support. Our findings suggest that cross-circulation should enable extended support and interventions in extracorporeal organs.

End-stage lung disease has a profound socioeconomic impact and remains the third leading cause of death worldwide[1,2]. Lung transplantation represents the only curative intervention. However, donor organ demand far exceeds supply[3], and due to stringent listing criteria, the actual demand is probably underestimated. Currently, four out of five donor lungs are deemed unacceptable for transplantation at the time of donation[4], making lung the least utilized solid organ and necessitating the increasing use of extracorporeal membrane oxygenation as a bridge-to-transplant for critically ill patients[4–8].

To address these challenges, there are major initiatives worldwide to increase the number of transplantable lungs, including the following. (1) Criteria expansion: the use of donors older than 55 years, or lungs donated following cardiac death[9–11]. (2) Extracorporeal devices: *ex vivo* lung perfusion (EVLP) to recondition marginally unacceptable donor lungs[12]. (3) Bioengineered lungs: tissue-engineering strategies utilizing stem cells and fully decellularized or bioartificial scaffolds[13–17] to develop functional lungs *de novo*. (4) Xenogeneic lungs: genomic and immunologic alterations to enable the xenotransplantation of swine or non-human primate lung[18,19], thereby providing a constant supply of donor organs. However, despite these efforts, the annual number of lung transplantations remains steady, and waitlist mortality continues to rise[3].

Among current approaches, EVLP may hold the greatest promise for immediate clinical impact. The utility of commercially available EVLP systems for recovery of marginally unacceptable donor lungs is under investigation in clinical trials[20,21], and several groups have already employed EVLP before lung transplantation[22–24]. Nevertheless, the number of lungs recovered using EVLP remains limited, and may be insufficient to meet the growing demand. Notably, clinical EVLP systems are approved to support lungs for up to 6 h (ref. [25]), a time too short for recovery of lungs beyond the marginally unacceptable range and for advanced therapeutic interventions (for example, pharmacotherapy, immunomodulation and gene/cell therapy). The physiologic limitations of EVLP can be attributed to the absence of systemic regulation (for example, renal, hepatic, pancreatic, neurohormonal). Even with repeated exchanges of perfusate, the loss of homeostasis in the extracorporeal lung inevitably leads to cellular damage, pulmonary oedema, impaired gas exchange and deterioration of lung function.

To overcome the limitations of EVLP, we developed a 'cross-circulation' platform using a clinically relevant swine model. Early attempts at cross-circulation between two humans utilized a healthy individual to support and augment the organ function of a patient suffering from a critical but potentially reversible illness given sufficient time for recovery[26–28] (for example, hepatic insufficiency, uraemia, eclampsia). In the present study, we investigated the use of cross-circulation between a recipient and an extracorporeal lung (Fig. 1a) via two experimental groups: (1) a prolonged maintenance group (Fig. 1a, upper left) to assess the feasibility of performing normothermic extracorporeal organ support for long enough to enable therapeutic intervention and (2) an ischaemic recovery group (Fig. 1a, lower left) to demonstrate the recovery of injured lungs in a clinically relevant model.

[1]Department of Biomedical Engineering, Columbia University Medical Center, Columbia University, New York, New York 10032, USA. [2]Department of Surgery, Columbia University Medical Center, Columbia University, New York, New York 10032, USA. [3]Department of Clinical Perfusion, Columbia University Medical Center, Columbia University, New York, New York 10032, USA. [4]Department of Pathology and Cell Biology, Columbia University Medical Center, Columbia University, New York, New York 10032, USA. [5]Institute of Comparative Medicine, Columbia University Medical Center, Columbia University, New York, New York 10032, USA. [6]Center for Human Development, Columbia University Medical Center, Columbia University, New York, New York 10032, USA. [7]Department of Medicine, Columbia University Medical Center, Columbia University, New York, New York 10032, USA. [8]Center for Translational Immunology, Columbia University Medical Center, Columbia University, New York, New York 10032, USA. [9]Department of Microbiology and Immunology, Columbia University Medical Center, Columbia University, New York, New York 10032, USA. †These authors contributed equally to this work. *e-mail: mb781@cumc.columbia.edu; gv2131@cvolumbia.edu

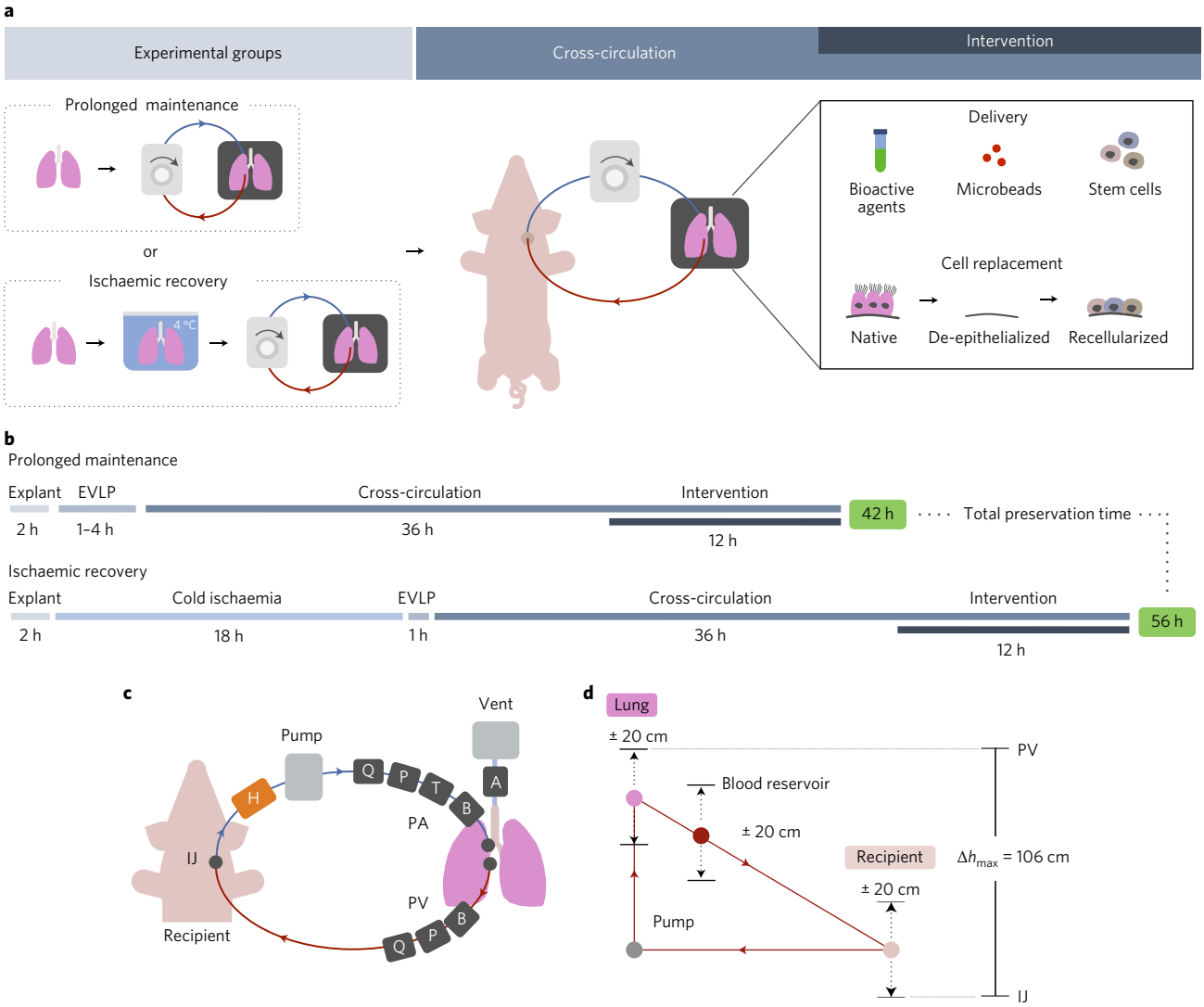

Figure 1 | Experimental procedure and extracorporeal lung maintenance strategy. a, Setup of interventional cross-circulation procedures. Lungs were explanted and, before cross-circulation, they were subjected to either isolated EVLP (prolonged maintenance group) or static cold ischaemia (ischaemic recovery group). **b**, Timelines of prolonged maintenance and ischaemic recovery experimental groups. **c**, Cross-circulation circuit diagram with integrated circuit elements. A, airflow probe; B, blood sample port; H, warm water jacket; IJ, internal jugular vein; P, pressure sensor; PA, pulmonary artery; PV, pulmonary vein; Q, flow probe; T, temperature probe. Extracorporeal lung perfusion and ventilation target parameters: PA pressure, <20 mmHg; PV pressure, 3–5 mmHg; flow, 0.2–0.4 l min^{-1} (5–10% of cardiac output); temperature, 36–38 °C; respiratory rate, 6–8 bpm; fraction of inspired oxygen (FiO_2), 40%. **d**, Use of height differences to modulate extracorporeal blood flow (red arrows) by circuit hydrostatic pressure differences.

Results

Pre-clinical swine model of cross-circulation. The procedure for establishing cross-circulation is outlined in Fig. 1a. Donor lungs were collected in the standard fashion[29,30], and the pulmonary artery (PA), pulmonary vein (PV) and trachea were cannulated (Fig. 2c). The challenge of collecting venous return from multiple pulmonary veins following removal of the left atrium (Fig. 2b) was managed via the implementation of a vascular bio-bridge (Fig. 2a) and a custom crenellated cannula (Fig. 2c, inset). Three-dimensional computational modelling of blood flow suggests laminar flow through the bio-bridge (Fig. 2d). Timelines for experimental groups are shown in Fig. 1b. In the prolonged maintenance group, a conventional EVLP circuit was primed with donor blood collected during lung harvest, and EVLP was initiated (Fig. 1a, upper left). In the ischaemic recovery group, lungs were maintained at 4 °C for 18 h before initiation of EVLP (Fig. 1a, lower left). In both experimental groups, a recipient swine was placed under general anaesthesia, and the internal jugular veins were cannulated and connected to the EVLP circuit to achieve cross-circulation between the recipient and the extracorporeal lung. After 24 h of normothermic cross-circulation support, multiple experimental interventions were demonstrated (Fig. 1a, right) until procedures were terminated as planned at 36 h of cross-circulation support.

Target parameters were defined for extracorporeal lung perfusion and ventilation for both experimental groups (Fig. 1). Integrated circuit elements (Fig. 1c) enabled real-time monitoring and maintenance of pressure, flow and temperature. In addition to feedback-regulated pressure-limited flow, modulation of the transpulmonary pressure gradient was achieved by precisely maintaining hydrostatic pressures by regulating the heights of the lung, blood reservoir and recipient (Fig. 1d). Thermal imaging confirmed that warm, freshly explanted lungs placed on ice (Fig. 2e, left) were efficiently cooled with cold flush (in keeping with standard transplantation protocol, Fig. 2e, middle), and warmed to normothermia following reperfusion (Fig. 2e, right) after transfer to the warm, humidified organ chamber (Supplementary Fig. 2d).

Haemodynamic stability of the recipient. The median weight of recipient animals ($n=6$) was 41.4 kg (range: 38.0–70.4 kg). Recipients were under general anaesthesia for an average of 40.1 ± 1.5 h. All recipients remained haemodynamically stable throughout the duration of cross-circulation support (Table 1, Fig. 3a and Supplementary Tables 1–3), in normal sinus rhythm, and without the need for vasopressor support. There were no significant differences between the respective baseline and end-point values for lactate (1.52 ± 0.49 mM and 0.71 ± 0.31 mM), pH (7.48 ± 0.07 and 7.36 ± 0.05), or the oxygen partial pressure, p_{O2} (530 ± 62 mmHg and 520 ± 81 mmHg). Haemolytic markers (lactate dehydrogenase, D-dimer, fibrinogen, plasma free haemoglobin) remained within normal ranges. Within each experimental group, no significant changes in serum levels of pro- or anti-inflammatory cytokines were detected between 0 and 36 h of cross-circulation (Fig. 3b,c). P-selectin, an indicator of platelet activation and endothelial injury, remained in the normal range throughout the entire procedure for both groups. M30, a marker of epithelial cell death, did not increase significantly in either experimental group (Fig. 3d). Pro-inflammatory cytokine levels were initially higher in the ischaemic recovery group and, with the exception of interleukin 1β (IL-1β) and tumour-necrosis factor-α (TNFα), trended downward over time (IL-6, IL-8, IL-17, angiotensin II). Although elevated in the ischaemic recovery group, all cytokine levels were within previously reported normal ranges (Supplementary Table 9). While the anti-inflammatory cytokine IL-10 increased over the first 12 h of cross-circulation before trending downward in the prolonged maintenance group, IL-10 levels were initially higher and remained

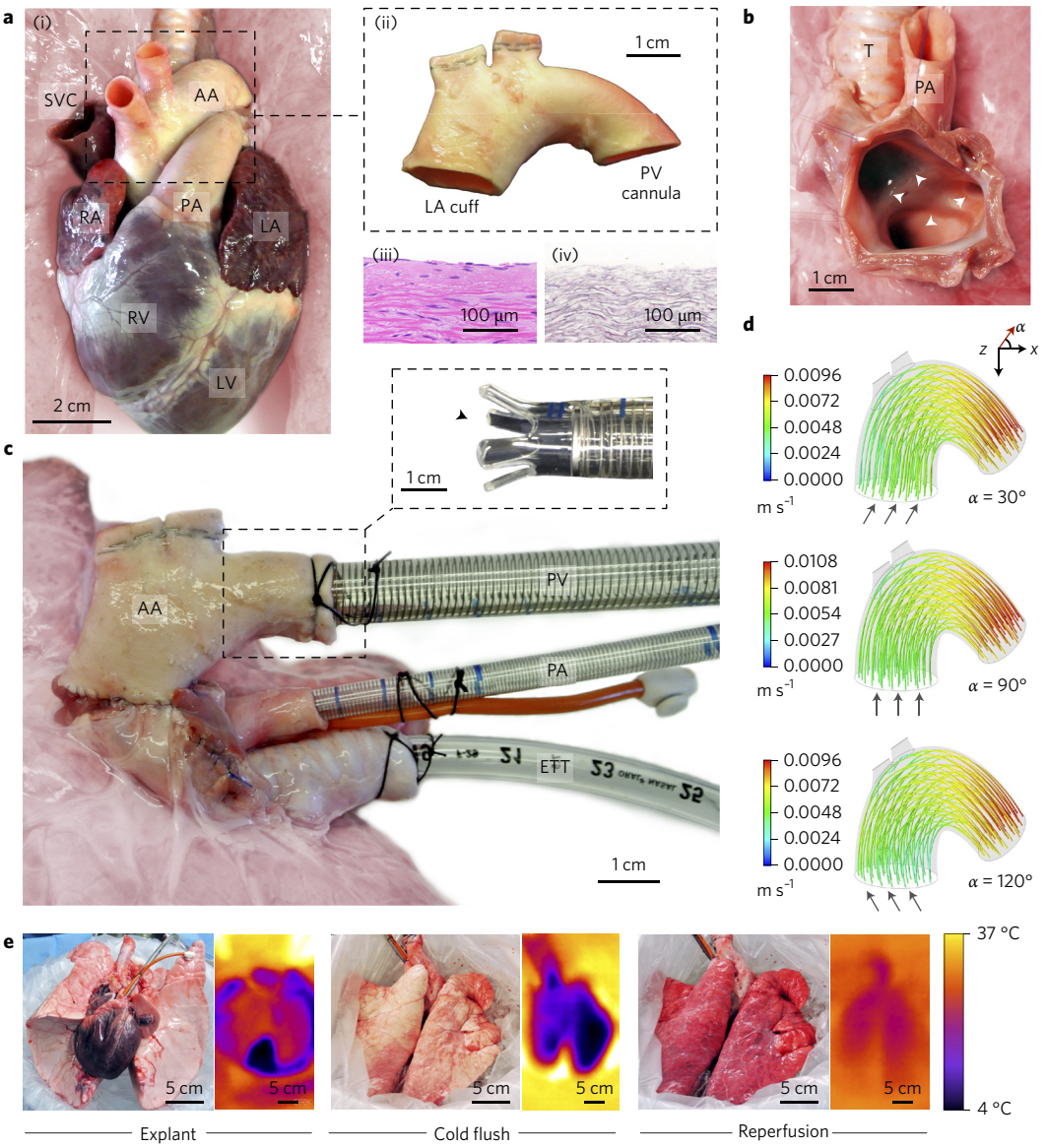

Figure 2 | Management of pulmonary venous drainage and utilization of donor vessel as a bio-bridge. a, Characterization of the bio-bridge. Aortic arch (AA) *in situ* (i). SVC, superior vena cava; RA, right atrium; RV, right ventricle; PA, pulmonary artery; LA, left atrium; LV, left ventricle. AA dissected, brachiocephalic and left subclavian branches stapled (ii). H&E staining of AA showing endothelialized lining of bio-bridge (iii). Silver stain of AA showing reticular fibres supporting bio-bridge wall (iv). **b**, Left atrial (LA) cuff after removal of the heart, revealing the pulmonary veins (arrowheads). T, trachea. **c**, Lung cannulation. AA serving as bio-bridge sutured into place with PA, PV cannulas and endotracheal tube (ETT). Inset: custom PV cannula with flared tip and crenellations (arrowhead). **d**, Three-dimensional computational model simulating blood flow entering the bio-bridge at varying angles. Blood flow streamlines obtained by computational fluid dynamic simulations at $\alpha=30°$, 90° and 120°. **e**, Thermal imaging of explanted donor lungs on ice (left), cold flush and transfer to normothermic organ chamber (middle), and re-perfusion with blood (right).

Table 1 | Recipient safety and stability throughout 36 h of cross-circulation support.

Time (h)	0	12	24	36
Haemodynamic stability				
Heart rate (bpm)	92 ± 25	85 ± 16	75 ± 18	78 ± 22
Systolic BP (mmHg)	92 ± 17	92 ± 13	100 ± 14	96 ± 17
Temperature (°C)	35.1 ± 1.0	36.2 ± 0.7	36.4 ± 0.5	36.2 ± 0.7
SpO_2 (%)	97 ± 1.8	98 ± 0.7	98 ± 1.2	97 ± 2.7
Haemogas				
pH	7.48 ± 0.07	7.43 ± 0.03	7.39 ± 0.04	7.36 ± 0.05
p_{O2} (mmHg)	530 ± 62	501 ± 54	522 ± 38	520 ± 81
p_{CO2} (mmHg)	39 ± 6.3	39 ± 5.5	47 ± 3.0	49 ± 1.8
HCO_3 (mM)	29 ± 2.0	26 ± 4.4	29 ± 2.4	28 ± 2.8
Biochemical analysis				
WBCs (10^9 l^{-1})	12.7 ± 4.2	12.5 ± 5.5	10.2 ± 1.9	9.9 ± 2.0
Platelets (10^9 l^{-1})	330 ± 62	310 ± 53	258 ± 36	229 ± 53
Hgb/Hct (g dl^{-1}/%)	6.8/22.6 ± 0.9/2.5	7.0/23.3 ± 1.2/3.8	6.6/22.0 ± 2.5/8.8	5.4/17.7 ± 1.2/3.7
AST/ALT (U l^{-1})	29/34 ± 9.2/9.1	60/33 ± 22.0/10.2	65/32 ± 17.3/9.6	254/42 ± 270/28
Creatinine (mg dl^{-1})	0.79 ± 0.14	0.78 ± 0.19	0.70 ± 0.20	0.72 ± 0.08
Lactate (mM)	1.52 ± 0.49	1.59 ± 0.67	0.79 ± 0.22	0.71 ± 0.31
Glucose (mg dl^{-1})	109 ± 35	110 ± 21	106 ± 17	92 ± 22
Haemolytic markers				
LDH (U l^{-1})	336 ± 63	382 ± 89	383 ± 67	397 ± 98
ACT (s)	-	301 ± 59	292 ± 61	274 ± 39

Values are for both experimental groups combined ($n = 6$). See Supplementary Table 1 for comparative values between prolonged maintenance ($n = 3$) and ischaemic recovery ($n = 3$) group recipients. All values represent mean ± standard deviation. WBCs, white blood cells; BP, blood pressure; Hgb, haemoglobin; Hct, haematocrit; AST, aspartate transaminase; ALT, alanine transaminase; LDH, lactate dehydrogenase; ACT, activated clotting time.

elevated throughout the 36 h of cross-circulation in the ischaemic recovery group (Fig. 3c).

Extracorporeal lung performance. Lung weight in the prolonged maintenance group did not change significantly (0 h, 0.48 ± 0.09 kg; 36 h, 0.43 ± 0.04 kg; $p > 0.05$), whereas lung weight in the ischaemic recovery group decreased significantly over the first 4 h of cross-circulation (0 h, 0.70 ± 0.05 kg; 4 h, 0.53 ± 0.08 kg; $p < 0.05$) and then remained stable over the remaining 32 h (4 h, 0.53 ± 0.08 kg; 36 h, 0.57 ± 0.04 kg; $p > 0.05$) (Fig. 4a). The trans-pulmonary pressure gradient was tightly maintained at 5–15 mmHg throughout all procedures ($n = 6$; Fig. 4b). No significant changes in pressure–volume loops (Fig. 4c, left) or dynamic compliance (Fig. 4d, left) were observed over 36 h of cross-circulation support in the prolonged maintenance group. However, in the ischaemic recovery group, derangement in pressure–volume loops (Fig. 4c, right) and a corresponding decrease in dynamic compliance (Fig. 4d, right) was seen at 12 h, followed by normalization of pressure–volume loops by 24 h and compliance values exceeding those at baseline by 36 h. Notably, the build-up of lactate[31,32] that occurred during the initial EVLP phase (before initiation of cross-circulation) of each experiment in the prolonged maintenance group (1.85 mM at 1 h, 8.20 mM at 2 h and 12.38 mM at 4 h) quickly normalized (<2.5 mM) following initiation of cross-circulation and remained within the normal range (Fig. 4e). In the prolonged maintenance group, extracorporeal lungs kept at a fraction of inspired oxygen (FiO_2) of 40% maintained a partial pressure arterial oxygen (PaO_2)of 315 ± 34 mmHg corresponding to a PaO_2/FiO_2 (P/F) ratio of 821 ± 102 mmHg (Fig. 4f, dashed line and Supplementary Fig. 8f,i). In the ischaemic recovery group, lungs had an initial average PaO_2 of 245.6 ± 133.7 mmHg corresponding to a P/F ratio of 614.16 ± 334.30 mmHg (Fig. 4f and Supplementary Fig. 8f,ii). Following an initial increase, all lungs experienced a slight decline in function until normalizing after 18 h. In response to the performance challenges of (1) increasing minute ventilation by 100% and (2) increasing FiO_2 from 40% to 100%, extracorporeal lungs demonstrated the ability to exchange gas as shown by differences (Δ) in baseline and challenge levels of pulmonary artery and vein haemogases (Fig. 4g): Δp_{O2} (oxygenation; Fig. 4h) and Δp_{CO2} (ventilation; Fig. 4i). Notably, lungs in the ischaemic recovery group did not achieve Δp_{O2} and Δp_{CO2} values equivalent to lungs in the prolonged maintenance group until after 24 h of cross-circulation.

Extracorporeal lung analysis: prolonged maintenance group. Donor lungs showed no apparent visual or bronchoscopic evidence of oedema (Fig. 5a,b). Histologic analysis (Fig. 5c, (i),(ii)), scanning (Fig. 5c, (iii)) and transmission electron microscopy (Fig. 5c, (iv)) revealed intact structural and cellular architecture in extracorporeal lungs after 36 h of cross-circulation support. Histologic staining revealed maintenance of important lung structures, including intact pseudostratified, columnar and cuboidal respiratory epithelium (Fig. 5d, (i),(v)); airway cilia (Fig. 5d, (ii)); and submucosal glands, airway cartilage and smooth muscle (Fig. 5d, (iv)); without signs of interstitial oedema or degradation of reticular (Fig. 5d, (iii)) or elastic fibres (Fig. 5d, (vi)) in the perialveolar extracellular matrix (Supplementary Fig. 4). Conducting airways were free of oedema and secretions, as observed by bronchoscopy after the 36 h of cross-circulation (Fig. 5b).

Assessment of extracorporeal lung metabolism showed a significant increase in metabolism over the first 24 h of cross-circulation support (Fig. 5e). The viability and function of type II pneumocytes was confirmed by uptake of boron-dipyrromethene-labelled surfactant protein B (BODIPY-SPB) delivered into the distal lung (Fig. 5f). Function of the pulmonary endothelium was confirmed by uptake of acetylated low density lipoprotein (LDL) in

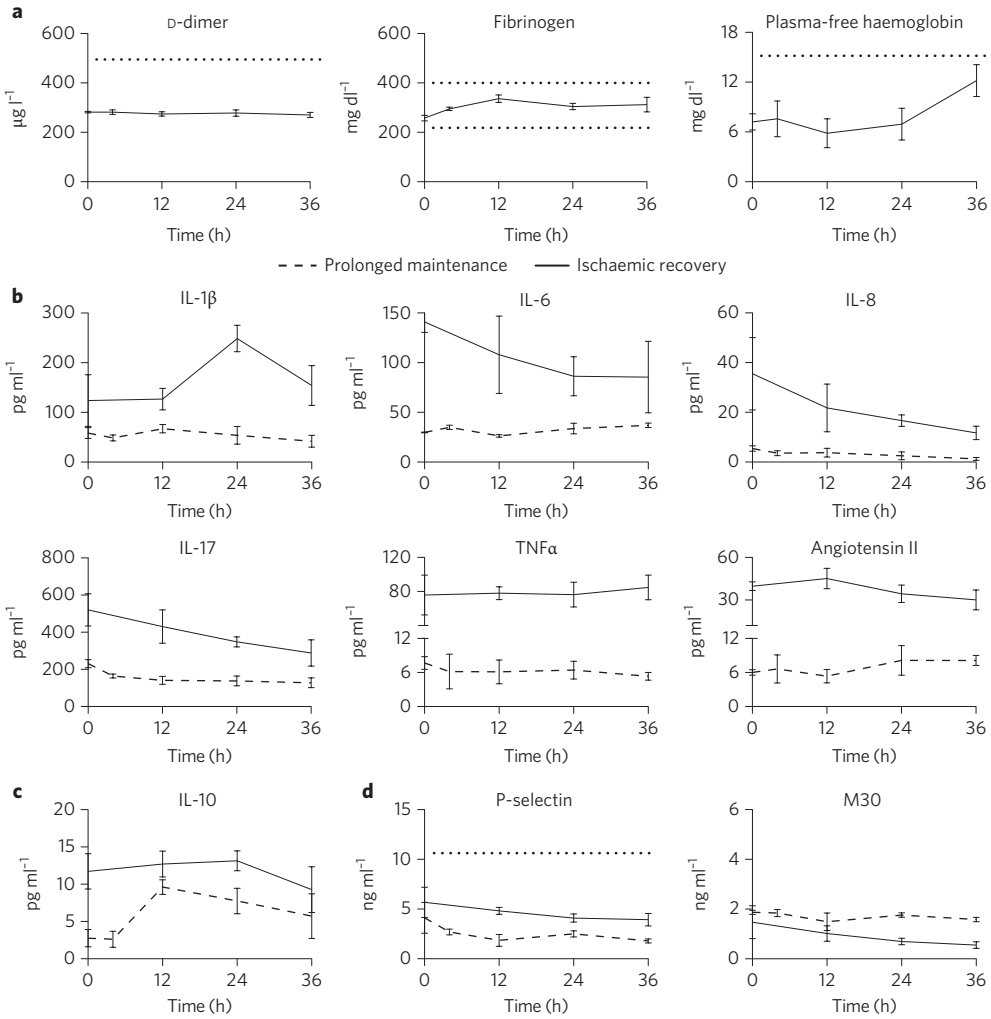

Figure 3 | Recipient safety and stability throughout 36 h of cross-circulation support. a, Haemolytic markers ($n=6$). **b**–**d**, Pro-inflammatory (**b**), anti-inflammatory (**c**) and activation markers (**d**) for recipients during prolonged maintenance ($n=3$) and ischaemic recovery ($n=3$). Dotted lines indicate upper and lower limits of fibrinogen and upper limits of D-dimer, plasma-free haemoglobin and P-selectin. No significant changes ($p>0.05$) in serum levels of pro- or anti-inflammatory cytokines or activation markers were detected between 0 and 36 h of cross-circulation for recipients in the prolonged maintenance or ischaemic recovery groups. All values represent the mean ± standard deviation.

pulmonary arterial endothelial cells (Fig. 5g). Vascular integrity was demonstrated by transmission electron microscopy analysis of small vessels (Supplementary Fig. 4c). CD31 immunostaining confirmed preservation of the pulmonary microvasculature, and immunostaining for tight junction protein 1 (ZO-1) confirmed retention of tight junction proteins in pulmonary capillaries and microvessels (Fig. 5i and Supplementary Fig. 8d,e). Increases by 6–9 mmHg in pulmonary artery and vein pressures were measured in response to epinephrine bolus at 36 h to confirm preservation of vasoresponsiveness to adrenergic stimulation (Fig. 5h).

Pathologic assessment of the extracorporeal lung was performed in a randomized blinded fashion to obtain lung injury scores (Supplementary Fig. 6a–c). Extracorporeal lungs were scored by quantification of marginalized neutrophils, early and late apoptotic cells, alveolar oedema and interstitial infiltrate (Supplementary Fig. 6d,g). Scores in individual categories were added to obtain composite lung injury scores at 0, 12 and 24 h of cross-circulation. There were no significant differences between the 0, 12 and 24 h time points in either individual or composite lung injury scores (Fig. 5j). To assess the immune response in the distal lung, interstitial and alveolar macrophages were quantified, and a significant decrease in those carrying the CD163 antigen ($p<0.001$) was found between initiation and 24 h of cross-circulation (Fig. 5k).

Extracorporeal lung analysis: ischaemic recovery group. Following 18 h of cold ischaemia, lungs demonstrated gross (Fig. 6a, upper), radiographic (Fig. 6a, middle) and thermographic (Fig. 6a, lower) evidence of consolidation, atelectasis and non-uniform perfusion (Supplementary Fig. 5a–c). Bronchoscopy at the initiation of cross-circulation revealed mild airway oedema (Fig. 6b and Supplementary Video 2) and abundant cellular content in bronchoalveolar lavage (BAL) fluid (Fig. 6d, upper). By 24 h of cross-circulation, airway oedema resolved, atelectatic lung was recruited, and lungs were uniformly perfused and remained normal up to 36 h, at which time fewer cells were observed in the BAL fluid (Fig. 6d, lower and Supplementary Video 1). Myeloperoxidase activity, an indicator of neutrophil activation, was elevated at 12 h but was significantly reduced by 36 h ($p<0.001$; Fig. 6c). Histologic analysis revealed neutrophil migration and extravasation into the interstitial space surrounding vessels and large airways from 0–12 h, with resolution by 36 h (Supplementary Fig. 5d). Following ischaemia-reperfusion, metabolism of extracorporeal lungs significantly increased over 24 h (Fig. 6e). Microscopic analysis revealed derangements in lung architecture at 0, 6 and 12 h, and intact structural and cellular architecture at 24 and 36 h (Supplementary Fig. 5j). Transmission electron microscopy showed denuded basement membrane with gaps between type I pneumocyte cell

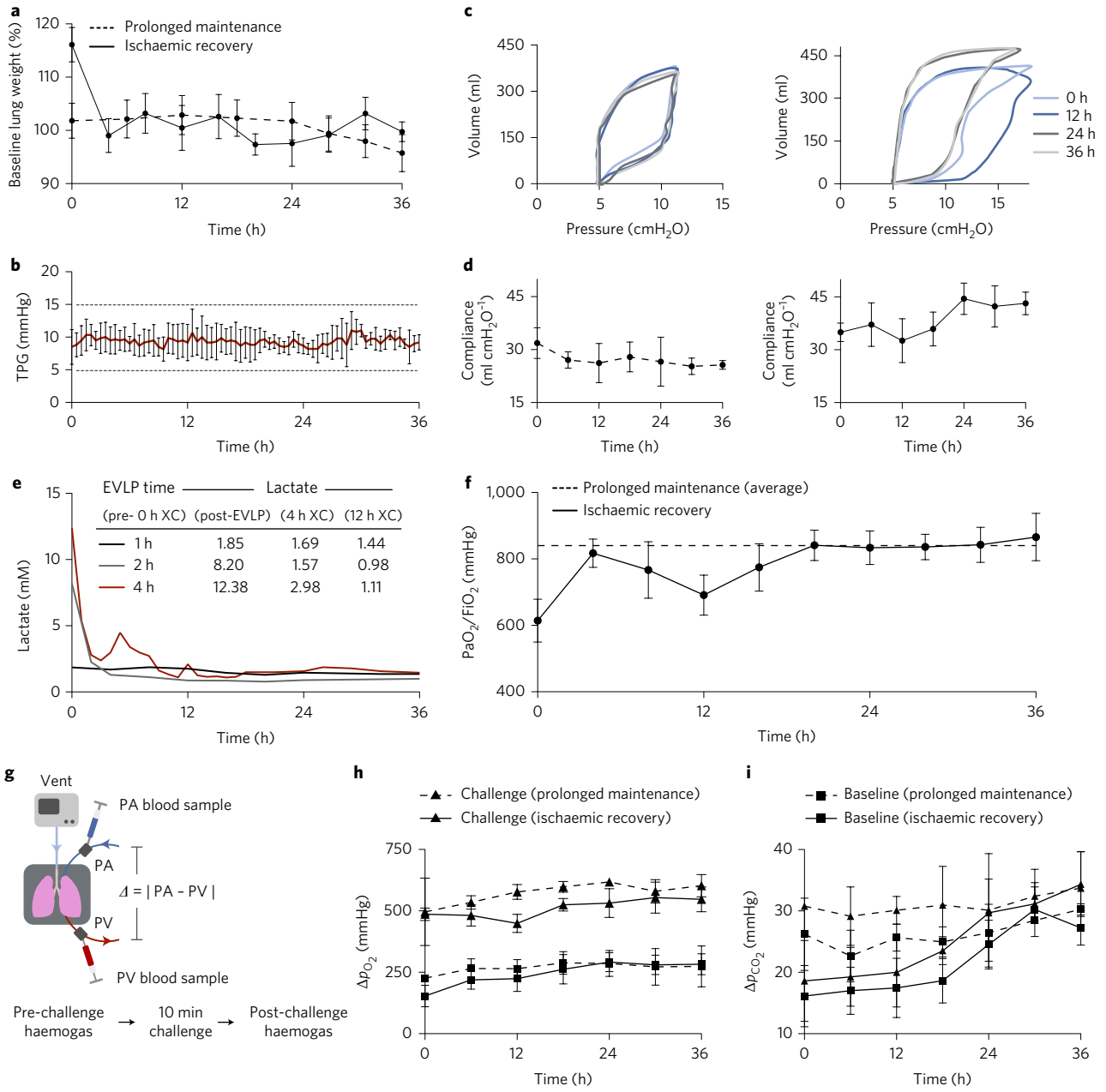

Figure 4 | Extracorporeal lung stability and performance during prolonged maintenance and ischaemic recovery. a, Percentage change of extracorporeal lung weight throughout cross-circulation procedure. **b**, Trans-pulmonary pressure gradient (TPG), the difference between PA and PV pressures ($n=6$). **c**, Pressure–volume loops during prolonged maintenance (left) and ischaemic recovery (right). **d**, Dynamic compliance during prolonged maintenance (left) and ischaemic recovery (right). **e**, Clearance of lactate over 36 h of cross-circulation (XC). Lactate accumulated over the course of 1, 2 and 4 h of EVLP before initiation of cross-circulation (*y* axis indicates lactate values at the end of EVLP and initiation of cross-circulation). **f**, PaO_2/FiO_2 ratios during prolonged maintenance and ischaemic recovery. **g**, Diagram of blood sampling before and after extracorporeal lung performance challenges, which were defined by adjustments made to ventilation (100% FiO_2 and 2× minute ventilation) every 4 h for 10-min periods to assess changes in p_{O2} and p_{CO2} in blood entering and exiting the extracorporeal lung. **h**,**i**, Responses in Δp_{O2} (**h**) and Δp_{CO2} (**i**) to 10-min challenges during prolonged maintenance and ischaemic recovery. All graphs represent data from the prolonged maintenance ($n=3$) and ischaemic recovery ($n=3$) groups. All values represent the mean ± standard deviation.

membranes at 0 and 12 h. By 24 and 36 h, the alveolar blood-gas barrier was shown to be intact (Fig. 6f and Supplementary Fig. 5e). A decrease in ZO-1 was observed at 0 and 12 h, with recovery by 36 h (Fig. 6g); at 36 h, ZO-1 staining was similar to that in healthy lungs. Randomized blinded pathologic lung injury scoring revealed a significant decrease in the composite lung injury score at 24 h (Fig. 6h). Quantification of macrophages carrying CD163 revealed a significant decrease in the total number of interstitial and alveolar macrophages between 12 and 24 h ($p<0.001$; Fig. 6i). Compared with lungs in the prolonged maintenance group, lungs in the ischaemic recovery group received higher composite lung injury scores at 0 and 12 h, with no difference in composite injury scores between the groups at 24 h (Fig. 6j).

Integrity of the pulmonary epithelium was assessed after 36 h of cross-circulation. Alcian blue staining and scanning electron microscopy of airway casts confirmed the maintenance of a

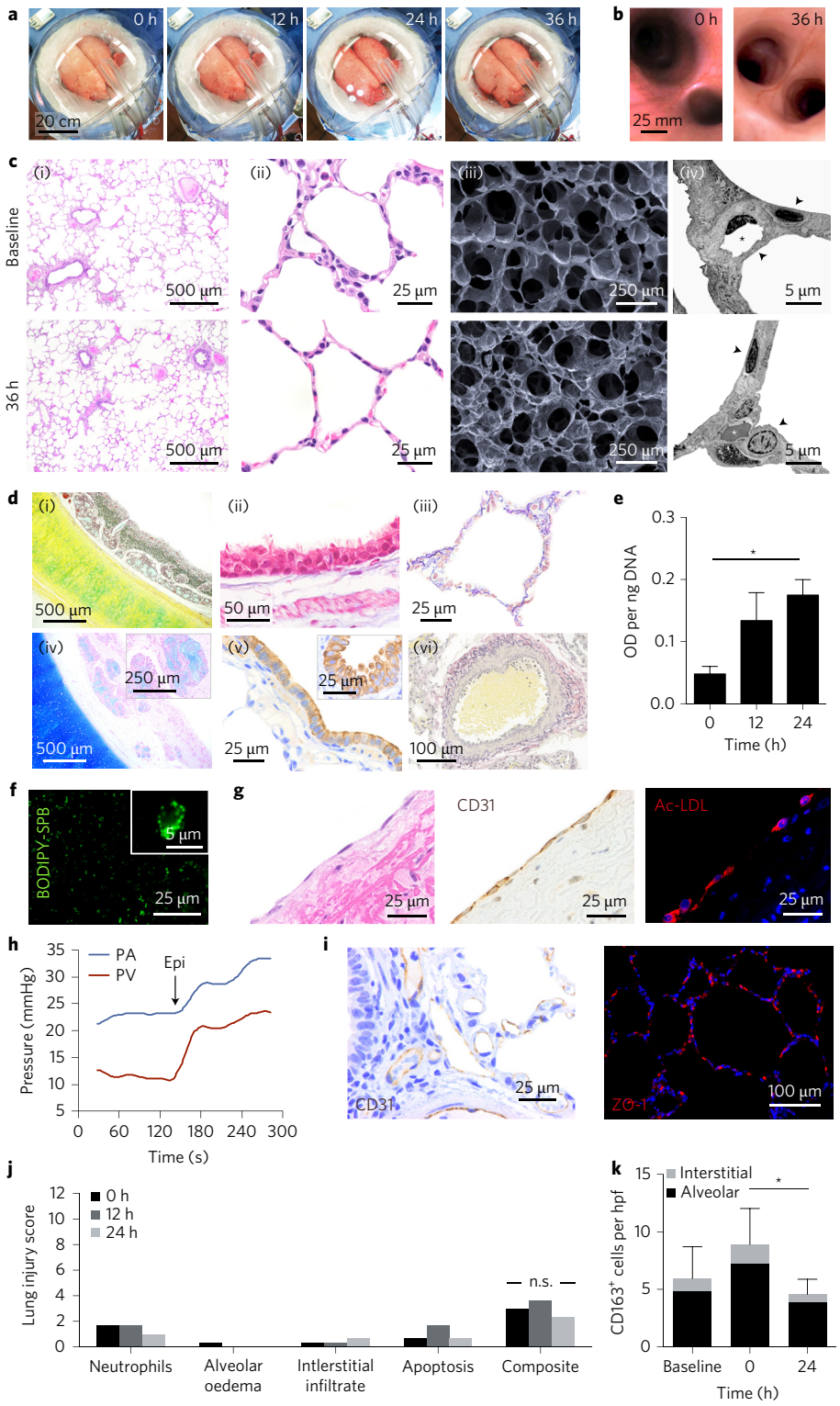

Figure 5 | Analysis of extracorporeal lungs in prolonged maintenance group. a, Macroscopic appearance of extracorporeal lungs throughout cross-circulation procedure. **b**, Airway bronchoscopy at baseline and 36 h endpoint. **c**, Baseline and 36 h H&E staining (i, ii), scanning electron microscopy (iii), and transmission electron microscopy (iv) with intact type I and II pneumocytes (arrowheads) and capillaries (asterisks). **d**, 36 h endpoint special or immunostaining: pentachrome (i), trichrome (ii), silver reticulin (iii), Alcian blue (iv), pan-cytoaeratin (v) and elastic von Gieson (vi). Insets of (iv) and (v) show a submucosal gland and pseudostratified airway epithelium, respectively. **e**, Metabolic activity of extracorporeal lung; $^{*}p < 0.001$. **f**, Functional analyses at 36 h endpoint: uptake of bronchoscopically delivered BODIPY-SPB by type II pneumocytes. Inset: single type II pneumocyte *in situ* with visible lamellar bodies. **g**, Uptake of acetylated LDL by pulmonary arterial endothelial cells carrying the CD31 antigen. Left, H&E; middle, CD31; right, acetylated LDL. **h**, Extracorporeal lung vasoresponsiveness following administration of epinephrine (epi) into the pulmonary artery after 36 h of cross-circulation. **i**, Integrity of microvascular endothelium by CD31 staining (left) and tight junctions by ZO-1 staining (right). **j**, Lung injury scoring. n.s., not significant. **k**, Macrophage quantification by CD163 immunostaining; $^{*}p < 0.01$. All graphs represent data from the prolonged maintenance group ($n = 3$). All values represent the mean ± standard deviation.

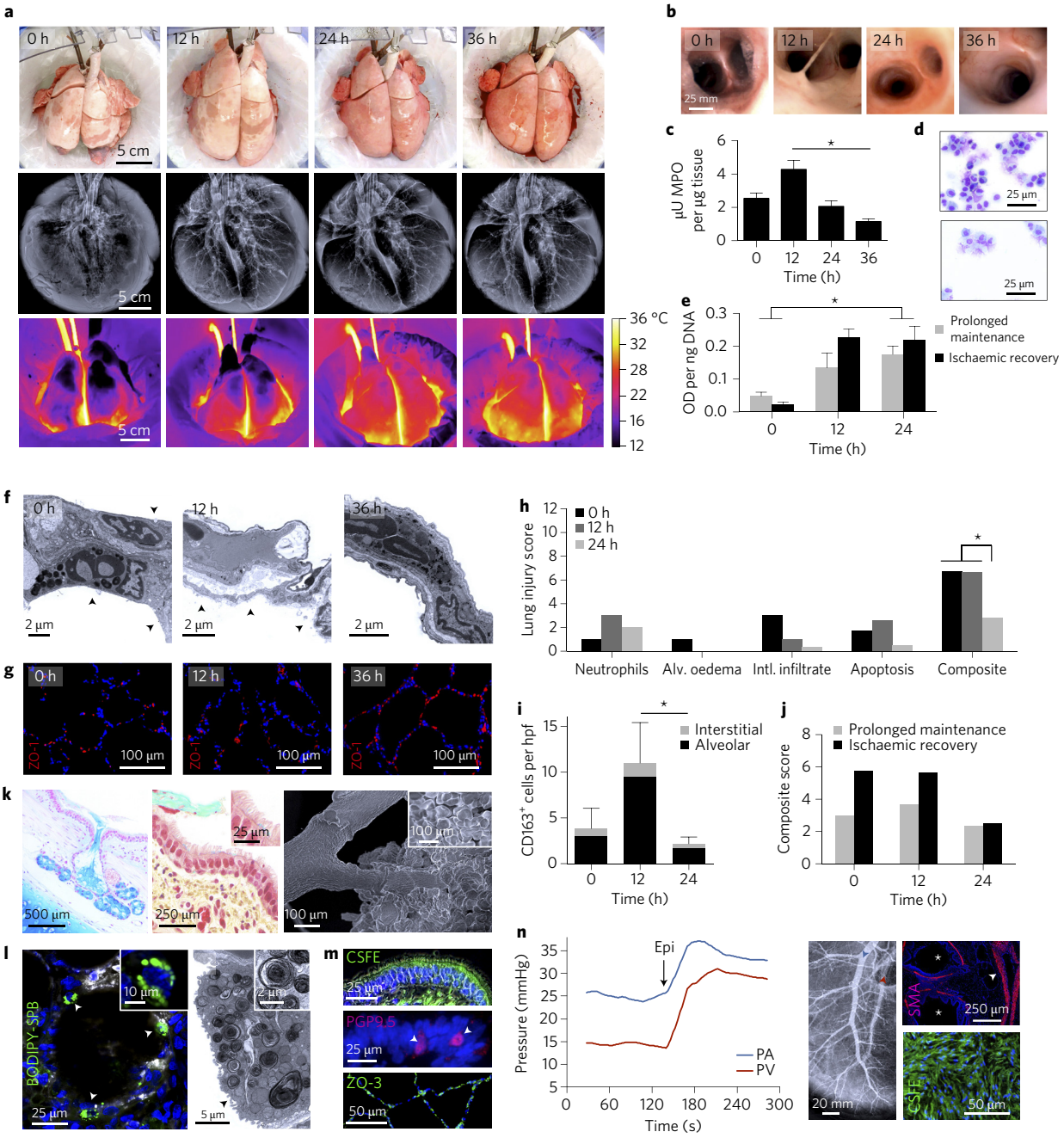

Figure 6 | Extracorporeal recovery and maintenance of injured lungs. a, Macroscopic analysis of injured lungs: gross appearance (upper), X-ray (middle) and thermal images (lower) throughout cross-circulation procedure. **b**, Analysis of pulmonary airways by bronchoscopy. **c**, Myeloperoxidase (MPO) activity in injured lungs throughout cross-circulation procedure; $^*p < 0.001$. **d**, Kwik-Diff staining of cells in BAL fluid at 0 h (upper) and 36 h (lower). **e**, Metabolic activity of extracorporeal lungs during prolonged maintenance and ischaemic recovery; $^*p < 0.001$. **f**, Transmission electron microscopy of injured lungs at 0, 12 and 36 h cross-circulation. Arrowheads indicate denuded alveolar basement membrane. **g**, ZO-1 (tight junction protein 1) immunostaining of pulmonary microvasculature at 0, 12 and 36 h of cross-circulation. **h**, Lung injury scoring. Alv., alveolar; Intl., interstitial. **i**, Macrophage quantification by CD163 immunostaining; $^*p < 0.01$. **j**, Composite lung injury scoring of prolonged maintenance and ischaemic recovery groups. **k**, Microscopic airway analysis of injured lungs after 36 h of cross-circulation: Alcian blue staining of secretory airway submucosal glands (left), pentachrome staining of intact columnar airway epithelium (middle) and airway cilia (inset), and scanning electron microscopy of airway cast of injured lungs after 36 h (right) with inset showing bifurcating bronchiole and alveolar sacs. **l**, Function and integrity of type II pneumocytes. Left: uptake of BODIPY-SPB at 36 h. Inset: single type II pneumocyte *in situ* with visible lamellar bodies. Right: transmission electron microscopy of secretory organelles and intact microvilli (arrowhead) in single type II pneumocyte. **m**, Integrity of the pulmonary airway epithelium of injured lungs after 36 h of cross-circulation: viability (CFSE), maintenance of pulmonary neuroendocrine cells (PGP9.5; arrowheads) and barrier function by alveolar epithelial tight junction protein 3 (ZO-3). **n**, Analysis of extracorporeal lung vasculature. Left: vasoresponsiveness following administration of epinephrine into the pulmonary artery after 36 h of cross-circulation. Middle: vascular integrity shown by X-ray following administration of radiocontrast dye (blue arrowhead, artery; red arrowhead, vein). Right upper: smooth muscle actin (SMA) immunostaining showing intact muscular layers surrounding vessels (arrowhead) and airways (asterisks). Right lower: uptake of CSFE by pulmonary artery endothelial cells confirming viability of the endothelial lining after 36 h. All graphs represent data from the ischaemic recovery group ($n = 3$). All values represent the mean ± standard deviation.

large-airway, bronchiolar and alveolar architecture, pseudostratified epithelium, and secretory function of submucosal mucous glands (Fig. 6k, left and right). Pentachrome staining revealed the presence of fully intact ciliated brush borders in large airways (Fig. 6k, middle). Live imaging of airway biopsies demonstrated viable cilia with coordinated beating, confirming functional preservation of the mucociliary escalator after 36 h of cross-circulation (Supplementary Video 4). Type II pneumocytes were visualized by transmission electron microscopy, and their viability and function at 36 h was confirmed by the uptake of fluorescently labelled BODIPY-SPB (Fig. 6l, left and right). Viability of pseudostratified epithelium in large airways was confirmed by the uptake of bronchoscopically delivered carboxyfluorescein succinimidyl ester (CSFE) at 36 h (Fig. 6m). Immunostaining for protein gene product 9.5 (PGP9.5) demonstrated maintenance of pulmonary neuroendocrine cells, and epithelial tight junction protein 3 (ZO-3) immunostaining suggested intact barrier function after 36 h of cross-circulation (Fig. 6m). The pulmonary vasculature was visualized by the injection of a radiocontrast dye at 36 h (Fig. 6n, middle). Viability of pulmonary arterial endothelial cells was confirmed by the uptake of CSFE (Fig. 6n, lower right), and smooth muscle actin immunostaining showed preservation of airway and vascular smooth muscle (Fig. 6n, upper right) after 36 h of cross-circulation. Increases by 9–15 mmHg in pulmonary artery and vein pressures were measured in response to an epinephrine bolus at 36 h (Fig. 6n, left), confirming vasoresponsiveness to adrenergic stimulation in a manner consistent with lungs in the prolonged maintenance group.

Assessment of airway inflammation. To assess the effect of cross-circulation on airway inflammation, BAL fluid was analysed for total protein and the inflammatory markers, interferon γ (IFNγ), IL-1β, IL-6, IL-8, IL-10, IL-17, M30 and TNFα. IFNγ was not detected at any time point in either experimental group. In the prolonged maintenance group, markers with no significant changes over 24 h of cross-circulation were total protein, IL-6 and M30. Significant increases were measured for IL-8 and IL-10, and significant decreases were measured for IL-1β, IL-17 and TNFα over 24 h of cross-circulation (Fig. 7a and Supplementary Fig. 8a). In the ischaemic recovery group, total protein and inflammatory cytokine levels were initially higher relative to the prolonged maintenance group, with the exception of IL-17. Total protein, IL-6, and TNFα increased significantly from 0 to 12 h and subsequently decreased significantly between 12 and 24 h (Fig. 7a and Supplementary Fig. 8b).

Demonstration of multiscale interventions in extracorporeal lungs. After 36 h of cross-circulation, a fluorescent cell viability marker (CFSE) was delivered with bronchoscopic guidance to targeted regions of the distal lung. Uptake of CFSE observed in all target regions (Fig. 7b, asterisks) confirmed cell viability at 36 h and demonstrated the potential for targeted delivery of therapeutics into the extracorporeal lung during cross-circulation.

The size of commercially available bronchoscopes limits their ability to access and visualize the distal lung. Because of the growing number of bronchopulmonary therapeutics[33–35] and the need to measure improvements in lung function, we developed a compact transpleural imaging system that enabled non-invasive, real-time surveillance of the lung and guided delivery of microbeads and fluorescently labelled porcine mesenchymal stem cells (MSCs) to the distal lung (Fig. 7c,d). Labelled MSCs were widely distributed throughout targeted regions of lung (Fig. 7e, (i),(ii)) and clearly seen in the alveoli and pulmonary interstitium (Fig. 7e, (iii)–(vii) and Supplementary Fig. 7a,b). Post-procedural analysis of MSCs showed co-localization with integrin-β1 (Fig. 7f and Supplementary Fig. 7c), an adhesion molecule known to mediate the migration of MSCs into the interstitium in multiple tissues[36].

To demonstrate the feasibility of replacing lung epithelium during cross-circulation, targeted bronchopulmonary segments were decellularized by micro-catheter delivery of 3-[(3-Cholamidopropyl) dimethylammonio]-1-propanesulfonate (CHAPS), a reagent previously used for lung decellularization[37,38]. Histologic comparison of intact (Fig. 7g, left) and de-epithelialized airways (Fig. 7g, middle) confirmed the removal of epithelium in large airways and alveoli, without disruption of adjacent large arteries, microvasculature or capillaries. Pentachrome staining suggested retention of extracellular matrix proteins including collagens and glycosaminoglycans (Fig. 7g, right (arrowheads) and Supplementary Fig. 7e), critical structural and biochemical factors for the proper attachment and function of newly delivered cells. The absence of haemorrhage, oedema and necrosis suggests that the regional decellularization process was well tolerated, and the stability and performance of the lung was unaffected. Decellularization was followed by delivery of pulmonary epithelial cells: heterogeneous populations of small airway epithelial cells and embryonic-stem-cell-derived alveolar progenitor cells were delivered to the large airways and distal alveoli, respectively, to replace the cells removed by decellularization. Small airway epithelial cells, delivered in a hydrogel made of lung extracellular matrix, were distributed across the airway surface and attached to the denuded basement membrane (Fig. 7h, upper and Supplementary Fig. 7f), while alveolar progenitors were observed throughout the alveoli (Fig. 7h, lower and Supplementary Fig. 7g).

Discussion

This first application of cross-circulation as a platform for prolonged normothermic extracorporeal organ support resulted in (1) the maintenance of viable extracorporeal lungs and stable recipients after 36 h of cross-circulation, and (2) the recovery of lungs subjected to ischaemia reperfusion injury.

The cross-circulation platform provided important benefits to the extracorporeal lung, and significantly extended the duration of normothermic support beyond what is currently achievable with EVLP. Recently published reports of prolonged preservation times include periods of cold ischaemia, and normothermic perfusion remains limited to a mean of 5.00 ± 0.93 h, with a mean total preservation time of 14.60 ± 1.82 h (ref. [39]). In the present study, we demonstrate that normothermic perfusion (EVLP + cross-circulation) can be extended to 37.67 ± 1.21 h, with total preservation time (cold ischaemia + normothermic perfusion) extending to 56.24 ± 0.11 h. Although cross-circulation support was terminated at 36 h to adhere to prescribed animal protocols, we postulate that cross-circulation could be extended to days or even weeks, an assumption currently being tested. Prolonging the duration further would allow for advanced therapeutic interventions not currently feasible; for example, gene/stem cell therapy, targeted cell removal/replacement, airway microbiome manipulation, bacterofection and donor–recipient immune modulation (Supplementary Fig. 1). Cross-circulation could serve as a platform for the recovery of organs that are unacceptable for transplantation, and could enable the assessment of graft function and modulation of the recipient response. This capability would allow for early recognition of primary graft dysfunction and for interventions prior to transplantation. Because this platform allows for continuous organ and recipient monitoring, it is well suited for studies of lung physiology, immunology and xenotransplantation.

Establishment of cross-circulation required the development of strategies to address challenges unique to prolonged extracorporeal organ support. Pulmonary venous drainage was managed using an endothelialized (that is, non-thrombogenic) bio-bridge between the pulmonary veins and the extracorporeal circuit, offering several key features as an alternative to artificial cuffs and gravity collection systems[40,41] (Supplementary Fig. 2f,iii). Pressure-limited flow allowed tight maintenance of a physiologic trans-pulmonary pressure gradient of between 5 and 15 mmHg throughout the duration of extracorporeal support, while height differences allowed for modulation of PV pressures via hydrostatic pressure differentials.

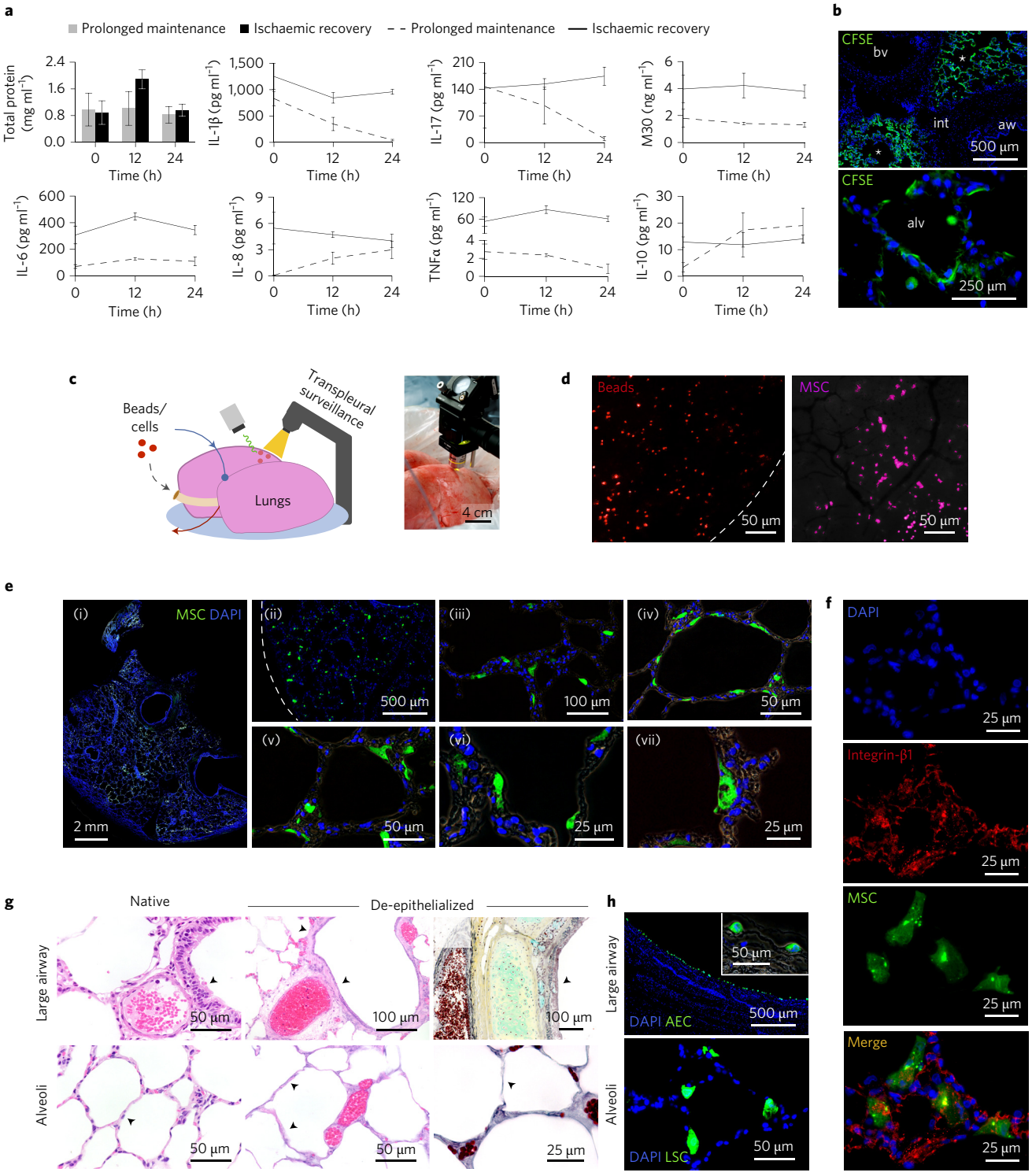

Figure 7 | Demonstration of multiscale interventions in extracorporeal lungs. a, Analysis of BAL fluid inflammatory markers during prolonged maintenance and ischaemic recovery. **b**, Delivery and uptake of cell viability marker (CFSE) in target regions of the distal lung (asterisks). No uptake was observed in blood vessels (bv), interstitium (int) or non-targeted proximal airways (aw). **c**, Transpleural imaging setup for non-invasive *in situ* imaging of microbeads and stem cells delivered to distal lung. **d**, Transpleural imaging following therapeutic delivery of microbeads and mesenchymal stem cells (MSCs). Dotted line represents pleura. **e**, Histologic analysis of delivered MSCs. Global distribution of MSCs throughout lung (i–iii). MSCs delivered in single cell suspension, localized in alveoli and interstitium (iv–vii). **f**, MSCs delivered in aggregate clusters, co-localized with integrin-β1. **g**, Histologic comparison of native and de-epithelialized lung. H&E staining showing removal of pseudostratified and squamous epithelium (arrowheads) in conducting airways (left) and alveoli (middle), with retention of intact pulmonary vasculature. Right: pentachrome stain with preservation of airway and alveolar basement membrane and extracellular matrix components including glycosaminoglycans (GAG, yellow/green), collagen (blue) and elastic fibres (black) in de-epithelialized regions. **h**, Cell replacement by targeted delivery of airway epithelial cells (AEC) into large airways (upper) using a lung matrix hydrogel carrier, and lung stem cells (LSC) into alveoli (lower). All graphs represent data from the prolonged maintenance ($n=3$) and ischaemic recovery ($n=3$) groups. All values represent the mean ± standard deviation.

In this study, the prolonged maintenance group consisted of healthy lungs that (1) served as proof that cross-circulation could support lungs outside the body at normothermia while preserving cell viability and global function for 36 h and (2) established recipient safety. In addition, lungs in the prolonged maintenance group served as healthy controls providing baseline values and trends over time for uninjured lungs on cross-circulation. To assess the ability of cross-circulation to recover damaged lungs in a clinically relevant injury model, lungs were subjected to ischaemia reperfusion injury followed by 36 h of cross-circulation (ischaemic recovery group). Lungs in the ischaemic recovery group were subjected to 18 h of static cold ischaemia, a period that is two to three times longer than what is accepted by most centres. Histologic evidence of cell and tissue derangement as a result of cold ischaemia was observed in separate injury validation studies and confirmed in blinded pathologic assessment of injured lungs (Supplementary Fig. 3).

Inflammation was assessed by analysis of inflammatory cytokines in the serum and BAL fluid. For markers of inflammation, lung pathologic scoring, lung metabolism and macrophage quantification, our analyses included time points up to 24 h to assess the effects of cross-circulation alone before any intervention in the extracorporeal lung (for example, decellularization and cell replacement). Preservation of lung integrity and function was demonstrated in the prolonged maintenance group throughout the entire duration of cross-circulation (Figs 4 and 5). For recipient serum markers, there were no significant differences over 24 h of cross-circulation (Fig. 3), underscoring the maintenance of homeostatic stability. Notably, BAL fluid analysis in the extracorporeal lung demonstrated a significant increase in anti-inflammatory IL-10 and significant decreases in pro-inflammatory IL-1β and IL-17. TNFα did not decrease significantly until after 12 h of cross-circulation, highlighting the value of prolonged recovery time. Although IL-8 increased, endpoint concentrations were 6–400 times lower than previously reported values (Supplementary Table 9).

In the ischaemic recovery group, lung weight and airway oedema were significantly reduced after 4–6 h of cross-circulation support (results that would be expected with an equivalent duration of EVLP; Figs 4a and 6b). However, a downward trend in several indicators of lung quality and function, such as dynamic compliance, P/F ratio and ZO-1, continued to decline in the first 12 h of cross-circulation before recovering to baseline values by 24 to 36 h (Fig. 4d, right panel; Figs 4f and 6h); thus highlighting the developmental nature of reperfusion injury and the importance of prolonged support time to enable recovery. Reperfusion injury is partly initiated by activated macrophages known to play a role in surfactant degradation[42] and in the rapid release of cytokines, most notably TNFα[43,44]. In the ischaemic recovery group, alveolar macrophages were highest at 12 h (Fig. 6j), corresponding to a decrease in lung compliance (Fig. 4d, right panel) and a significant increase in BAL levels of TNFα at the same time (Fig. 7a and Supplementary Fig. 8b). By 24 h macrophages and TNFα levels were significantly decreased, and compliance improved.

Neutrophils perpetuate the late phase of reperfusion injury (after 4 h of reperfusion) by increasing oxidative stress[45]. In the ischaemic recovery group, the increased presence of marginated neutrophils between 0 and12 h, and the subsequent decrease between 24 and 36 h, was confirmed by haematoxylin and eosin (H&E) staining (Supplementary Fig. 5d) and blinded pathologic assessment, quantified by neutrophil elastase immunostaining (Supplementary Fig. 6e), and assessed via myeloperoxidase activity (Fig. 6c). Furthermore, decreased ventilatory function, blinded pathologic assessment, analysis by transmission electron microscopy and reduced ZO-1 immunostaining all indicated that cellular derangement occurred throughout the first 12 h.

Beyond 12 h of cross-circulation, injured lungs recovered cellular and structural integrity and showed significant improvements at the cell and tissue level as well as in global function. Comprehensive analyses of recovered lungs (Figs 4 and 6) revealed the following: gross appearance, radiography and thermography consistent with healthy lungs; absence of airway secretions, and interstitial and alveolar oedema; restoration of barrier function with intact alveolar epithelium and epithelial and vascular tight junctions; recovery of cellular and structural integrity that was histologically consistent with healthy lungs; maintenance of airway structures including cartilage, smooth muscle and submucosal glands; and viability and function of the mucociliary escalator, pulmonary epithelial cells and vascular endothelial cells. Taken together, these data underlie a global lung function that resulted in P/F ratios >800 mmHg (values similar to those in healthy lungs) after 56 h outside the body.

Beyond prolonged normothermic extracorporeal support, cross-circulation may also enable interventions not currently feasible *ex vivo*. Targeted micro-volume delivery techniques[46] and the development of a radiation-free, real-time transpleural imaging systems enabled directed region-specific interventions rather than whole lung decellularization or treatment strategies. We demonstrated global, single-lobe and subsegmental delivery and engraftment of MSCs in both single-cell and aggregate suspensions. Given the large number of clinical trials of MSC therapy, cross-circulation may offer opportunities to improve delivery techniques and further investigate the engraftment and function of therapeutic stem cells over time.

There are several limitations to the present study: (1) While the use of inbred swine reduced immunological interactions, thus enabling this initial proof-of-concept study, future work will investigate prolonged cross-circulation between unrelated donor and recipient swine kept on immunosuppression. (2) While this study investigated lungs subjected to ischaemia reperfusion injury, ongoing studies are assessing the ability of cross-circulation to rescue severely damaged lungs in a gastric aspiration model. (3) Swine recipients were healthy at baseline. We envision that patients with end-stage lung disease on extracorporeal membrane oxygenation support awaiting lung transplantation may be candidates for clinical applications of cross-circulation. Initial candidates will probably be those with isolated lung disease (for example, interstitial lung disease) capable of handling the additional metabolic demand of an extracorporeal lung (~5% of total body metabolism)[47]. Before the implementation of cross-circulation, ethical considerations such as patient safety, informed consent, training and credentialing of providers, and outcome analysis would need to be addressed in a manner that is consistent with medical standards. (4) While flow in the extracorporeal lung was maintained at 5–10% of cardiac output, future studies should include ramp-up strategies to reach 40% of cardiac output. (5) Lungs maintained and recovered by cross-circulation were not transplanted. Future studies will investigate the effect of extended cross-circulation support on early and late outcomes following lung transplantation.

An intervention of increasing interest is cell replacement[48,49], whereby damaged or diseased cells are removed and replaced with healthy cell progenitors or differentiated cells. We demonstrated removal and replacement of the pulmonary epithelium in a targeted region-specific manner while maintaining the overall function and integrity of the lung (Fig. 7g,h and Supplementary Fig. 7e–g). To better control cell delivery into proximal airways, a hydrogel prepared from lung extracellular matrix was used as a natural carrier of airway cells. Our novel transpleural imaging system (Supplementary Fig. 9) enabled real-time visualization of cells during delivery and confirmed distribution, localization, and enabled monitoring over time without tissue sampling (Supplementary Video 3). Notably, this device has the potential to facilitate basic research and translational applications and to direct clinical interventions as a theranostic for image-guided delivery of therapeutic agents to distal regions of the lung not accessible by conventional bronchoscopy.

Patient-derived cell therapies offer exciting opportunities for the engineering of chimeric organs and may ultimately reduce the burden of immunosuppressive therapy and the incidence of chronic rejection. On the basis of the results reported here, we envision that cross-circulation could be applied to other transplantable organs, bioengineered grafts and xenotransplantation models (Supplementary Fig. 1b).

Methods

Animals. Twelve miniature swine (six donor–recipient pairs) were used in this study. Matched pairs of animals with well-defined major histocompatibility complex (MHC) loci were selected from a herd of partially inbred swine; selective breeding methods and detailed immunogenetic characteristics of this herd have been previously described[50]. Animals were 5–7 months of age, with a median weight of 40.2 kg (range, 38.2–47.3 kg) in the prolonged maintenance group, and a median weight of 43.8 kg (range, 38.0–70.4 kg) in the ischaemic recovery group. The study received approval from the Institutional Animal Care and Use Committee (IACUC) at Columbia University. All animal care and procedures were conducted in accordance with the US National Research Council's Guide for the Care and Use of Laboratory Animals, 8th edn.

Donor lung harvest. Donor pigs ($n=6$) underwent general anaesthesia via intramuscular induction with Telazol (5 mg per kg of body weight (hereafter, kg^{-1}); Zoetis) and buprenorphine hydrochloride (0.03 mg kg^{-1}; Hospira), and maintenance with continuous intravenous infusions of fentanyl citrate (0.1 mg kg^{-1} h^{-1}; West-Ward), midazolam (1.5 mg kg^{-1} h^{-1}; Akorn), and inhaled isoflurane (1–5% in oxygen; Henry Schein). Cefazolin (30 mg kg^{-1}; WG Critical Care) was given intravenously prior to skin incision and median sternotomy. A bolus of heparin (30,000 U) was intravenously administered (Sagent), and a cannula was placed and secured in the main pulmonary artery. Autologous blood was withdrawn and collected in citrate-phosphate-dextrose collection bags (Chinook Medical) and stored at 8 °C. Once a non-perfusing rhythm was observed, a cold anterograde low-potassium dextran flush (Perfadex, Vitrolife) with alprostadil (25 mg kg^{-1}; Prostin VR Pediatric, Pfizer) was administered, and the appendage of the left atrium was cut. Topical cooling was applied, the lungs were inflated to a sustained airway pressure of 15 cmH_2O, and the trachea was stapled (Endo GIA device; Medtronic). The heart and lungs were explanted en-bloc and placed on ice on a sterile back table.

In each donor swine, the heart was removed, leaving behind a circumferential left atrial cuff with a height of 3–5 mm. A cold retrograde flush with Perfadex (20 ml kg^{-1}) was then performed. The aortic arch was dissected free and the brachiocephalic and left subclavian branches were stapled or suture ligated. A 3–4 cm section of aorta was left on either side of these vessels to facilitate placement of the PV cannula on one end and attachment to the left atrial cuff on the other.

Lung storage for prolonged cold ischaemia. Lungs in the ischaemic recovery group ($n=3$) were placed in a sterile isolation bag with 500 ml of Perfadex. That bag was then placed in a second sterile isolation bag containing 1 l of normal saline and immediately placed on ice at 4 °C. The median duration of cold ischaemia was 18.6 h (range, 18.1–18.95 h). Lungs in the prolonged maintenance group ($n=3$) were immediately cannulated and started on conventional EVLP.

Lung cannulation and conventional EVLP of the donor lung. The aortic arch, acting as a bio-bridge, was connected to the left atrial cuff with a running 6-0 prolene suture (Ethicon), and a 36F crenellated venous drainage cannula was secured in place with a 2-0 Ti-Cron tie (Covidien). An 18–20F pulmonary artery cannula was secured in place with a purse-string 5-0 prolene suture and TourniKwik tourniquet (Medtronic). The trachea was cannulated with a 7.5 mm cuffed endotracheal tube (Sheridan). A 1 l bag of cold normal saline was used to flush the lungs and remove air from inside the PA and PV cannulas. A top-loading balance (Denver Instrument Company) and a double-lined warm saline-filled organ basin were placed in the preservation chamber (XVIVO Organ Chamber; XVIVO). The lungs were then placed in the basin in prone position, and the cannulas were secured. The circuit was primed with whole blood collected during donor harvest, de-aired and connected to the extracorporeal lung. Initial flow rates were set to 5–10% of the estimated cardiac output, with a target PA pressure of <15 mmHg and PV pressure of 3–5 mmHg.

The circuit and lungs were allowed to acclimate to ambient temperature, and ventilation was initiated within the first 10 min of conventional EVLP, with the following initial settings: volume control mode; respiratory rate, 6–8 bpm; tidal volume (TV), 6–8 ml kg^{-1}; positive end-expiratory pressure (PEEP), 5 cmH_2O; and FiO_2, 40% (Oxylog 3000 plus; Dräger). Atelectatic lung regions were recruited by increasing TV and PEEP (up to 10 cmH_2O), and by performing inspiratory hold manoeuvres (up to 25 cmH_2O). Manual recruitment was used if ventilation strategies failed to fully recruit all areas of the lung. Thermal images of the lung were captured at selected time points throughout the duration of study using a Seek Thermal XR camera or a FLIR T430sc infrared camera. Continuous time-lapse photography (1 frame min^{-1}) was performed using a Hero4 Black 4K camera (GoPro; Supplementary Video 1). EVLP ranged in time from 1–4 h in the prolonged maintenance group as a demonstration of the need for homeostatic regulation. EVLP duration in the ischaemic group lasted 30–60 min. To maximize safety, vascular leaks, air entrapment or circuit problems were addressed at this stage, before connection to the recipient.

Cross-circulation. Recipient pigs ($n=6$) underwent sedation and general anaesthesia in a similar fashion to donor pigs. Cefazolin (30 mg kg^{-1}) was given prior to skin incision and the pig was re-dosed every 8 h. A femoral arterial line (Arrow International) was placed for haemodynamic monitoring and periodic blood sampling. Bilateral neck cut-downs exposed the right and left internal jugular veins. A 15,000 U heparin bolus was administered, and cannulation with 18F catheters was performed in the standard fashion using the Seldinger technique. Immediately before the initiation of cross-circulation, recipient pigs were intravenously administered 1 g of methylprednisolone (APP Pharmaceuticals) and 500 mg of calcium chloride (Hospira). Donor blood used to prime the circuit during EVLP was not removed. As shown in the circuit (Supplementary Fig. 2b,c), the tubing was spliced to connect the recipient pig to the conventional EVLP circuit, marking the start of cross-circulation.

Circuit elements consisted of a main console (Jostra HL-20 pump console; Maquet), disposable pump (Rotaflow centrifugal pump; Maquet), a soft shell reservoir (Maquet) and three-eighth inch tubing (Smart coated tubing; LivaNova). Pressure (PA and PV), flow (PA and PV) and temperature data were continuously monitored and recorded (VIPER clinical interfacing software; G2 v1.26.4; Spectrum Medical). Throughout the duration of cross-circulation, the recipient was maintained on a continuous heparin infusion (initial rate of 25 U kg^{-1} h^{-1}). Activated clotting time was measured using a HemoChron whole blood microcoagulation system (Accriva Diagnostics), and the heparin drip was adjusted to maintain a target value of 250–350 s. Physiological parameters of the recipient, including heart rate, electrocardiogram, blood pressure (cuff and arterial A-line pressure), mean arterial pressure (MAP), oxygen saturation (SpO_2), end-tidal CO_2, temperature, and respiratory rate, were continuously monitored and recorded using a multi-parameter Advisor vital signs monitor (SurgiVet).

Blood analysis. *Recipient monitoring.* Blood samples were drawn from the femoral A-line every hour. Blood gas analysis was performed using an epoc point-of-care blood analysis system (Epocal). Additional samples were collected in test-specific specimen vials (BD Vacutainer) every 4 h and sent to the laboratory (Antech Diagnostics, New Hyde Park, NY, USA) for complete blood count, basic metabolic panel, liver function tests, lactate dehydrogenase, and coagulation panels. Additional haemolytic markers (D-dimer, fibrinogen, plasma free haemoglobin) and inflammatory markers (angiotensin II, IL-1β, IL-6, IL-8, IL-10, IL-17, M30, P-selectin, RAGE, TNFα and IFNγ) were analysed using commercially available enzyme-linked immunosorbant assays (ELISAs), in triplicate, according to the manufacturer's instructions. A list of the ELISA kits used is provided in Supplementary Table 6.

Extracorporeal lung monitoring. Blood samples were drawn from the PA cannula (blood entering the lungs) and PV cannula (blood exiting the lungs) every hour and analysed in the same fashion as recipient samples. Temporary changes in ventilation settings (minute ventilation and FiO_2) were made in order to further assess extracorporeal lung performance every 4 h. Immediately following this challenge period, a second set of blood samples were drawn from the PA and PV cannulas (Supplementary Tables 7 and 8). Dynamic compliance (C_{dyn} = TV/(PIP − PEEP); ml per cmH_2O; PIP, peak inspiratory pressure) of the extracorporeal lung was calculated every 4 h. Pressure and volume recordings of the lung were measured using a custom-configured measurement system consisting of sensors and an acquisition device (Arduino Uno). Data collected via this system were processed and pressure–volume loops were generated using MATLAB v.R2016b (Mathworks). Lung weight was obtained every 4 h using a scale (Denver Instrument Company) housed inside the organ chamber. The basin and contents were tared (zeroed) at each time point to ensure accurate recordings. X-ray images of the lung were acquired using a PXP-16HF portable X-ray unit (United Radiology Systems) at 2.2 mA s and 90 kVp. A 15–20 ml injection of Optiray 320 (Medtronic) was administered to evaluate the vascular network integrity of the lung at the end of the experiment.

BAL analysis. Sample collection was performed by wedging a 3.8 mm flexible bronchoscope (Ambu aScope3) into a subsegmental bronchus of the right or left lung. Normal saline (10 ml) was injected twice, aspirated, and then collected in a sterile specimen trap (Busse Hospital Disposables). Specimens were centrifuged at 3,500 rpm for 10 min at 4 °C. Snap-frozen supernatants were stored at −80 °C until further processing. Inflammatory markers (IL-1β, IL-6, IL-8, IL-10, IL-17, M30, P-selectin, RAGE, TNFα and IFNγ) were analysed using commercially available enzyme-linked immunosorbant assays (ELISAs), in a similar fashion to the blood samples. BAL total protein concentrations were determined using a protein assay

(Pierce Coomassie Bradford Protein Assay kit, Thermo Fisher) with bovine serum albumin as the standard. Smears of BAL fluid were allowed to dry on glass coverslips and then stained using a commercially available Shandon Kwik-Diff kit (Thermo Fisher) according to manufacturer's instructions. Slides were imaged as previously described.

Functional assays. *Acetylated LDL uptake.* To assess the vascular endothelium[51], at the end of each experiment, biopsies of the left and right pulmonary artery and sections of pulmonary veins were collected and placed in a 96-well plate (BD Falcon). Acetylated LDL, Alexa Fluor 594 conjugate (Thermo Fisher, L35353) was diluted 1:200 in DMEM/F12K (50/50) cell culture media (Corning). Media alone (control; 150 µl) was added to wells containing vascular biopsies from each source. The remaining wells received 150 µl of media containing acetylated LDL. The multi-well plate was covered with aluminium foil and incubated at 37 °C with gentle shaking for 4 h. Following incubation, samples were washed five times with PBS buffer, fixed in cold phosphate-buffered 4% paraformaldehyde for 48 h, embedded in paraffin, and sectioned at 5 µm thickness. Following de-paraffinization and DAPI staining, slides were examined using a fluorescence microscope (Olympus FSX100).

BODIPY-surfactant uptake. To assess the viability and functional uptake of type II pneumocytes[52], fluorescent BODIPY-labelled surfactant protein B (BODIPY-SPB) was delivered into the distal lung using a Renegade microcatheter system (Boston Scientific) and a flexible bronchoscope. After 30 min, a surgical stapler with medium/thick reloads (Triple-Staple Technology; Medtronic) was used to collect lung samples. Samples were dissected, rinsed in DPBS buffer, and imaged immediately with an Olympus FSX100 microscope. Enhanced resolution was obtained by incubating 36 h lung tissue specimens (2 mm × 2 mm) with 20 ng ml^{-1} BODIPY-SPB for 30 min at room temperature. Specimens were stained with CellMask Deep Red plasma-membrane stain for 10 min, followed by five washings with DPBS for 1 min each. Images were taken with a two-photon confocal laser scanning microscope (Leica TCS SP8). Visualization of the fluorescence signal in a speculated pattern (lamellar bodies) within type II pneumocytes indicated surfactant uptake.

Vasoconstriction/responsiveness test. The effect of catecholamine stimulation on pulmonary vascular tone was tested after 36 h of cross-circulation. Epinephrine (4 mg; International Medication Systems) was intravenously administered into the PA cannula of the extracorporeal lung. PA and PV pressure and flow were continuously recorded, as previously described, to assess the changes in pulmonary artery and vein pressures (and thus the trans-pulmonary pressure gradient) in response to the adrenoceptor-mediated effect of epinephrine. Recipient haemodynamic and physiologic monitoring continued throughout the duration of study. To confirm that the response was isolated to the lung and not affected by haemodynamic changes in the recipient, the test was repeated with the lung decoupled from cross-circulation while on isolated EVLP.

Metabolic activity assay. To assess changes in lung metabolism, lung tissue from randomly selected wedge samples was collected after 0, 18 and 36 h of cross-circulation. Parenchymal samples (approximately 250 µl in volume; $n = 6$) were dissected in a sterile fashion, finely minced, gently homogenized and placed in a 96-well plate. AlamarBlue assay[53] (Thermo Fisher) reagent was diluted 1:10 in DMEM cell culture media with 10% foetal bovine serum, and 100 µl of AlamarBlue was added to wells containing lung sample homogenates. AlamarBlue alone (100 µl) was added to wells containing no lung homogenate (negative controls). The multi-well plate was covered with aluminium foil and incubated at 37 °C with gentle shaking for 2 h. Following incubation, well contents were transferred into new 96-well plates, and absorbance was measured at 570 nm and normalized to 600 nm. Following the metabolic activity assay, the DNA content of each sample was quantified using Quanti-iT PicoGreen dsDNA Assay kit (Invitrogen) according to the manufacturer's instructions. Samples were digested in 250 µg ml^{-1} papain at 60 °C for 4 h and mixed with PicoGreen reagent. Fluorescence emission was measured at 520 nm with excitation at 480 nm, and DNA was quantified using a standard curve.

Myeloperoxidase activity assay. To study the activity of myeloperoxidase, a peroxidase enzyme most abundant in neutrophil granulocytes, lung tissue samples were collected at multiple time points throughout the cross-circulation procedure. Small tissue sections (≥10 mg) were immediately snap frozen in liquid nitrogen and stored at −80 °C. Once all time point samples were collected, the assay was conducted according to the manufacturer's instructions (Abcam, ab111749).

Live cilia imaging. To visualize the presence of cilia and assess their function, large airway sections were collected following 36 h of cross-circulation. Specimens were dissected into small pieces (2 mm × 2 mm) and placed lumen-side-down onto a 50 mm glass-bottom dish (MatTek). Tissue was immersed in a 1:100 microbead (0.2 µm) suspension in PBS. A SecureSlip coverslip (Grace Bio-Labs) was placed on top of the sample. Remaining suspension outside the area of the coverslide was gently aspirated using a pipette. Images were acquired using an inverted Olympus IX81 microscope with an Andor Zyla 5.5 sCMOS camera at 100 frames s^{-1} and NIS Elements Advanced Research software (Nikon). The methods were adapted from previously described imaging techniques in rodents[54].

Immunohistochemical staining. Lung sections were de-paraffinized, subjected to boiling citrate buffer (pH 6.0) for antigen retrieval and blocked with 10% normal goat serum in PBS for 2 h at room temperature. Primary antibodies were added and incubated for 12 h at 4 °C or 4 h at room temperature. For all stains, the secondary antibody was diluted 1:200 and incubated for 1 h at room temperature. Sections were mounted in Vectashield Mounting Medium with DAPI (Vector Laboratories), coverslipped, and imaged with an Olympus FSX100 microscope. Late apoptosis was detected on tissue sections using a TUNEL (TdT-mediated dUTP nick end-labelling) assay. Additional stains for neutrophil elastase, pan-cytokeratin, caspase-3, CD163 and CD31 were conducted by the Herbert Irving Comprehensive Cancer Center molecular pathology services at Columbia University. A list of antibodies and dilutions used is provided in Supplementary Table 5.

Histopathologic analysis. *Sample collection.* Before starting the experiment, the location of each lung wedge sample was randomized for each time point. The lung was divided into 16 regions as shown in Supplementary Fig. 6a, and a random number generator (http://www.random.org) was used to assign a lung region to each sample collection time point to avoid sampling bias. A surgical stapler with medium/thick reloads was used to obtain lung samples every 4 h. Specimens were immediately fixed in cold phosphate-buffered 4% paraformaldehyde for 48–72 h, embedded in paraffin, and sectioned at 3 µm or 5 µm thickness. All sections were stained for H&E and examined via light microscopy. Additional sections were stained for silver reticulin, Alcian blue (pH 2), elastic van Gieson, trichrome and pentachrome by the histology service of the Department of Molecular Pathology at Columbia University.

Blinded pathologic review. A pulmonary pathologist blinded to the study protocol and experimental groups evaluated slides (H&E and immunohistochemical staining for neutrophil elastase, TUNEL and caspase-3) from the 0, 12 and 24 h timepoints of all cross-circulation experiments (prolonged maintenance, ischaemia trials and ischaemic recovery; Supplementary Fig. 6b). All slides were randomized, arbitrarily numbered and delivered to the pathologist without reference to experimental time points or conditions[55]. To evaluate the extracorporeal lung at each time point, a modified lung injury score was developed from previously described methods[56,57]. Scoring was based on alveolar oedema (0 ⇒ <5% of all alveoli had oedema fluid, 1 ⇒ 6–25%, 2 ⇒ 26–50%, 3 ⇒ >50%), interstitial infiltrate (lymphocytes and neutrophils in the interstitium around vessels and airways and in alveolar septa and pleura (1 ⇒ <50 per high-power field (hpf), 2 ⇒ 50–100 per hpf, 3 ⇒ >100 per hpf), neutrophils per 5 hpf (×40; 0.2 mm^2; 0 ⇒ <5, 1 ⇒ 6–10, 2 ⇒ 11–20, 3 ⇒ >20), and total number of apoptotic cells per 5 hpf (×40; 0.2 mm^2; 0 ⇒ <2, 1 ⇒ 3–5, 2 ⇒ 6–10, 3 ⇒ >10) (Supplementary Fig. 6c). Numbers for early and late apoptosis, as quantified by caspase-3 and TUNEL, were combined into a single score. The sum of individual scores yielded a total lung injury score ranging from 0 to 12 as an index of lung maintenance and injury at each experimental time point.

Electron microscopy. *Scanning electron microscopy.* Lung samples obtained at cross-circulation times of 0 and 36 h were fixed in formalin, rinsed in 70% ethanol, frozen and lyophilized. Airway castings were obtained at 36 h using a commercially available anatomical corrosion kit (Batson's #17, Polysciences) according to the manufacturer's instructions. Sections were imaged on a Hitachi S-4700 FE-SEM or a Zeiss GeminiSEM 300 with an accelerating voltage of 2.5 kV.

Transmission electron microscopy. Lung samples obtained at cross-circulation times of 0 and 36 h were fixed with 2.5% glutaraldehyde in 0.1 M Sorenson's buffer (pH 7.2). Samples were then post-fixed with 1% OsO_4 in Sorenson's buffer for 1 h. After dehydration, tissues were embedded in Lx-112 (Ladd Research Industries). Thin sections were cut on the PT-XL ultramicrotome at 60 nm thickness. The sections were stained with uranyl acetate and lead citrate and examined under a JEOL JEM-1200 EXII electron microscope. Images were captured with an ORCA-HR digital camera (Hamamatsu) and recorded using the AMT Image Capture Engine v.602.569.

Therapeutic delivery into extracorporeal lung. *Decellularization of target lung regions.* Decellularization of target lung regions (removal of lung epithelium, with endothelial preservation) was accomplished by delivering decellularization solution through the airway. A mild detergent solution containing 8 mM CHAPS (Sigma), 0.5 M NaCl (Sigma) and 25 mM EDTA (Sigma) was introduced bronchoscopically into targeted bronchopulmonary segments by a custom micro-catheter delivery system. Immediately following withdrawal of the bronchoscope, a 4–7F Fogarty occlusion catheter (Edwards Lifesciences) was inflated and left in place to prevent escape of decellularization fluid from the targeted region. Decellularization

solution was allowed to dwell for 4 h before repeated bronchoalveolar lavage with sterile normal saline. To assess the effectiveness of decellularization, lung wedge samples were collected following decellularization and before further intervention, fixed, embedded, de-paraffinized, and imaged, as previously described.

Delivery of mesenchymal stem cells. Porcine adipose-derived MSCs were isolated from three different donor animals (mature Yucatan mini-pigs; 21–32 months old; 48–73 kg or a mean of 60.0 ± 7.9 kg). Subcutaneous fat (~20 g) was collected from the dorsal abdominal area of each animal ($n = 3$), and the adipose-derived stem cells were isolated as previously described[58]. MSCs were cultured in DMEM, 10% foetal bovine serum, 1% penicillin/streptomycin and 0.1 ng ml^{-1} basic fibroblast growth factor, and expanded up to passage 3 before use. At the time of the experiment, passage-3 cells were trypsinized, counted using a Countess automated cell counter (Invitrogen), and re-suspended in PBS at a final concentration of 3–30 × 10^6 cells ml^{-1} for labelling with CSFE (Abcam) or CellBrite NIR790 cytoplasmic membrane dye (Biotium) according to the manufacturers' instructions.

Cell delivery was performed using a 3.8 mm flexible bronchoscope with a 1.2 mm lumen for therapeutic delivery and intervention. Labelled cells in suspensions of single-cell or 5–10 cell aggregates were delivered either globally (from above the carina) or locally into targeted lobes or segments. For single-cell delivery, cells were delivered within 15 min of suspension and gentle rocking was maintained prior to delivery. For 5–10 cell aggregates, cells were allowed to settle without rocking for up to 30 min, delivery was completed once aggregates were confirmed by microscopy. Timing of MSC delivery was varied experimentally (at 20, 24 or 26 h of cross-circulation). Subsequent live transpleural imaging of near-infrared-labelled cells was performed using a custom imaging system developed in our lab that consists of an LED excitation source (M780L3, Thorlabs), a camera (Zyla 4.2, Andor Technology) and an objective (Plan N 10×, Olympus) (Supplementary Fig. 9). Images and videos acquired with the system were processed using NIS-Elements Advanced Research or ImageJ v.1.43u (National Institutes of Health) (Supplementary Video 3). To assess the distribution, attachment and migration of CSFE-labelled MSCs, lung wedge samples were collected from all lobes at the end of the experiment, fixed, embedded, de-paraffinized and imaged as previously described, using an Olympus BX61VS virtual slide microscope.

Delivery of CSFE and fluorescent microbeads. To demonstrate the feasibility of targeted delivery of fluid micro-volumes into the distal lung, CFSE (Affymetrix, eBioscience) was reconstituted in dimethyl sulfoxide at a concentration of 1.06 M and protected from light. Fluorescent microbeads (FluoSpheres F-8834, Life Technologies; excitation/emission, 580/605 nm; diameter, 10 µm) were suspended in PBS at a final concentration of 10^6 beads ml^{-1}. At determined experimental time points, either CFSE or microbeads were delivered into the airways with a flexible bronchoscope and Renegade microcatheter system. Following delivery, microbeads were imaged transpleurally using the imaging system described above, using a 595 nm LED (M595L3, Thorlabs) as the excitation source. To assess the distribution and uptake of CSFE, lung wedge samples were collected at the end of the experiment, fixed, embedded, de-paraffinized and imaged, as previously described.

Delivery of human airway epithelial cells and human embryonic stem cell-derived alveolar progenitor cells. Following decellularization, shake tests of BAL fluids were conducted to confirm the removal of residual detergent before the introduction of cells. Human airway epithelial cells (Lonza, Allendale) or human embryonic stem cell-derived alveolar progenitor cells (derived from Rockefeller University Embryonic Stem Cell Line 2; NIH approval number, NIHhESC-09-0013; registration number, 0013; passage 13-24; negative for mycoplasma) were cultured as previously described[59]. Cultured cells were passaged by trypsinization, labelled with CFSE according to the manufacturer's instructions, and suspensions were prepared at a concentration of 5–10 × 10^6 cells ml^{-1}. Cells were then suspended in a lung-specific extracellular matrix hydrogel (TissueSpec Matrix Hydrogel; MatriTek) and delivered either proximally to decellularized airways or distally to decellularized regions of the respiratory zone. Delivery of cells occurred after 24 h of cross-circulation to allow sufficient time for cell distribution and attachment. To assess the distribution and attachment of delivered cells, lung wedge samples were collected at the conclusion of the experiment, fixed, embedded, de-paraffinized, and imaged, as previously described.

Statistical analysis. One-way analysis of variance test with Tukey's multiple comparison *post hoc* tests and Student's *t*-tests were performed using Prism v.6 (GraphPad). A value of $p < 0.05$ was considered statistically significant.

Study design. The study was designed as a pilot study ($n = 6$) for the purposes of testing procedures and demonstrating proof of concept for a 36 h cross-circulation procedure. Our hypothesis was (1) extracorporeal lungs could be maintained with cross-circulation support for 36 h and (2) lungs subjected to prolonged cold ischaemia could be recovered. The study was conducted with the minimum number of animals to achieve reproducibility and statistical significance between time points. Data from this initial study will be used to conduct power analysis for subsequent investigations. Collection of all samples was performed as technical replicates in triplicate.

Randomization of sampling. Samples of extracorporeal lung collected for histologic, microscopic, and pathologic analyses were collected randomly during procedures according to a pre-determined lung map (Supplementary Fig. 6a) with 16 regions arbitrarily numbered by a random number generator (http://www.random.org).

Blinded review. All analytical assessments were blinded to the maximum practical extent. Pathologic analysis was performed by an independent expert to eliminate bias.

Data availability. The authors declare that all data supporting the findings of this study are available within the paper and its Supplementary Information.

Received 31 July 2016; accepted 25 January 2017; published 6 March 2017

References

1. Rabe, K. F. *et al.* Global strategy for the diagnosis, management, and prevention of chronic obstructive pulmonary disease: GOLD executive summary. *Am. J. Respir. Crit. Care Med.* **176,** 532–555 (2007).
2. Kochanek, K. D., Murphy, S. L., Xu, J. & Arias, E. Mortality in the United States, 2013. *NCHS Data Brief* **178,** 1–8 (2014).
3. Valapour, M. *et al.* OPTN/SRTR 2013 annual data report: lung. *Am. J. Transplant.* **15,** 1–28 (2015).
4. Ware, L. B. *et al.* Assessment of lungs rejected for transplantation and implications for donor selection. *Lancet* **360,** 619–620 (2002).
5. Pomfret, E. *et al.* Solving the organ shortage crisis: the 7th annual American Society of Transplant Surgeons' State-of-the-Art Winter Symposium. *Am. J. Transplant.* **8,** 745–752 (2008).
6. Klein, A. *et al.* Organ donation and utilization in the United States, 1999–2008. *Am. J. Transplant.* **10,** 973–986 (2010).
7. Javidfar, J. & Bacchetta, M. Bridge to lung transplantation with extracorporeal membrane oxygenation support. *Curr. Opin. Org. Transplant.* **17,** 496–502 (2012).
8. Fuehner, T. *et al.* Extracorporeal membrane oxygenation in awake patients as bridge to lung transplantation. *Am. J. Respir. Crit. Care Med.* **185,** 763–768 (2012).
9. Bittle, G. J. *et al.* The use of lung donors older than 55 years: a review of the United Network of Organ Sharing database. *J. Heart Lung Transplant.* **32,** 760–768 (2013).
10. Van Raemdonck, D. *et al.* Lung donor selection and management. *Proc. Am. Thorac. Soc.* **6,** 28–38 (2009).
11. Elgharably, H., Shafii, A. E. & Mason, D. P. Expanding the donor pool: donation after cardiac death. *Thorac. Surg. Clin.* **25,** 35–46 (2015).
12. Cypel, M. & Keshavjee, S. Extending the donor pool: rehabilitation of poor organs. *Thorac. Surg. Clin.* **25,** 27–33 (2015).
13. Rosen, C. *et al.* Preconditioning allows engraftment of mouse and human embryonic lung cells, enabling lung repair in mice. *Nat. Med.* **21,** 869–879 (2015).
14. Wagner, D. E. *et al.* Can stem cells be used to generate new lungs? *Ex vivo* lung bioengineering with decellularized whole lung scaffolds. *Respirology* **18,** 895–911 (2013).
15. Petersen, T. H. *et al.* Tissue-engineered lungs for *in vivo* implantation. *Science* **329,** 538–541 (2010).
16. Ott, H. C. *et al.* Regeneration and orthotopic transplantation of a bioartificial lung. *Nat. Med.* **16,** 927–933 (2010).
17. Wobma, H. & Vunjak-Novakovic, G. Tissue engineering and regenerative medicine 2015: a year in review. *Tissue Eng. Part B Rev.* **22,** 101–113 (2016).
18. Cooper, D. K. *et al.* Clinical lung xenotransplantation—what donor genetic modifications may be necessary? *Xenotransplantation* **19,** 144–158 (2012).
19. Laird, C., Burdorf, L. & Pierson, R. N. III Lung xenotransplantation: a review. *Curr. Opin. Org. Transplant.* **21,** 272–278 (2016).
20. Popov, A.-F. *et al. Ex vivo* lung perfusion–state of the art in lung donor pool expansion. *Med. Sci. Monit. Basic Res.* **21,** 9–14 (2015).
21. Mohite, P. *et al.* Utilization of the Organ Care System Lung for the assessment of lungs from a donor after cardiac death (DCD) before bilateral transplantation. *Perfusion* **30,** 427–430 (2015).
22. Cypel, M. *et al.* Normothermic *ex vivo* lung perfusion in clinical lung transplantation. *N. Engl. J. Med.* **364,** 1431–1440 (2011).
23. Zych, B. *et al.* Early outcomes of bilateral sequential single lung transplantation after *ex-vivo* lung evaluation and reconditioning. *J. Heart Lung Transplant.* **31,** 274–281 (2012).
24. Wallinder, A. *et al.* Transplantation of initially rejected donor lungs after *ex vivo* lung perfusion. *J. Thorac. Cardiovasc. Surg.* **144,** 1222–1228 (2012).
25. Warnecke, G. *et al.* Normothermic perfusion of donor lungs for preservation and assessment with the Organ Care System Lung before bilateral transplantation: a pilot study of 12 patients. *Lancet* **380,** 1851–1858 (2012).

26. Eschbach, J. Jr, Hutchings, R., Meston, B., Burnell, J. & Scribner, B. A technique for repetitive and long-term human cross circulation. *ASAIO J.* **10,** 280–284 (1964).
27. Burnell, J. *et al.* Observations on cross circulation in man. *Am. J. Med.* **38,** 832–841 (1965).
28. Burnell, J. *et al.* Acute hepatic coma treated by cross-circulation or exchange transfusion. *N. Engl. J. Med.* **276,** 935–943 (1967).
29. Saxena, P. *et al.* Procurement of lungs for transplantation following donation after circulatory death: the Alfred technique. *J. Surg. Res.* **192,** 642–646 (2014).
30. Sundaresan, S., Trachiotis, G. D., Aoe, M., Patterson, G. A. & Cooper, J. D. Donor lung procurement: assessment and operative technique. *Ann. Thorac. Surg.* **56,** 1409–1413 (1993).
31. Sanchez, P. G., Bittle, G. J., Burdorf, L., Pierson, R. N. & Griffith, B. P. State of art: clinical *ex vivo* lung perfusion: rationale, current status, and future directions. *J. Heart Lung Transplant.* **31,** 339–348 (2012).
32. Roman, M. *et al.* Comparison between cellular and acellular perfusates for *ex vivo* lung perfusion in a porcine model. *J. Heart Lung Transplant.* **34,** 978–987 (2015).
33. Lee, J. W., Fang, X., Gupta, N., Serikov, V. & Matthay, M. A. Allogeneic human mesenchymal stem cells for treatment of *E. coli* endotoxin-induced acute lung injury in the *ex vivo* perfused human lung. *Proc. Natl Acad. Sci. USA* **106,** 16357–16362 (2009).
34. Cypel, M. *et al.* Functional repair of human donor lungs by IL-10 gene therapy. *Sci. Transl. Med.* **1,** 4ra9 (2009).
35. Inci, I. *et al.* Reconditioning of an injured lung graft with intrabronchial surfactant instillation in an *ex vivo* lung perfusion system followed by transplantation. *J. Surg. Res.* **184,** 1143–1149 (2013).
36. Veevers-Lowe, J., Ball, S. G., Shuttleworth, A. & Kielty, C. M. Mesenchymal stem cell migration is regulated by fibronectin through α5β1-integrin-mediated activation of PDGFR-β and potentiation of growth factor signals. *J. Cell Sci.* **124,** 1288–1300 (2011).
37. O'Neill, J. D. *et al.* Decellularization of human and porcine lung tissues for pulmonary tissue engineering. *Ann. Thorac. Surg.* **96,** 1046–1056 (2013).
38. Petersen, T. H., Calle, E. A., Colehour, M. B. & Niklason, L. E. Matrix composition and mechanics of decellularized lung scaffolds. *Cells Tissues Organs* **195,** 222–231 (2011).
39. Yeung, J. C. *et al.* Outcomes after transplantation of lungs preserved for more than 12 h: a retrospective study. *Lancet Respir. Med.* **5,** 119–124 (2016).
40. Steen, S. *et al.* Transplantation of lungs from non–heart-beating donors after functional assessment *ex vivo*. *Ann. Thorac. Surg.* **76,** 244–252 (2003).
41. Cypel, M. *et al.* Technique for prolonged normothermic *ex vivo* lung perfusion. *J. Heart Lung Transplant.* **27,** 1319–1325 (2008).
42. Kitsiouli, E., Nakos, G. & Lekka, M. E. Phospholipase A 2 subclasses in acute respiratory distress syndrome. *Biochim. Biophys. Acta* **1792,** 941–953 (2009).
43. Maxey, T. S. *et al.* Tumor necrosis factor-α from resident lung cells is a key initiating factor in pulmonary ischemia-reperfusion injury. *J. Thorac. Cardiovasc. Surg.* **127,** 541–547 (2004).
44. Zhao, M. *et al.* Alveolar macrophage activation is a key initiation signal for acute lung ischemia-reperfusion injury. *Am. J. Physiol. Lung Cell Mol. Physiol.* **291,** L1018–L1026 (2006).
45. Eppinger, M. J., Jones, M. L., Deeb, G. M., Bolling, S. F. & Ward, P. A. Pattern of injury and the role of neutrophils in reperfusion injury of rat lung. *J. Surg. Res.* **58,** 713–718 (1995).
46. Kim, J., O'Neill, J. D., Dorrello, N. V., Bacchetta, M. & Vunjak-Novakovic, G. Targeted delivery of liquid microvolumes into the lung. *Proc. Natl Acad. Sci. USA* **112,** 11530–11535 (2015).
47. Loer, S. A., Scheeren, T. W. & Tarnow, J. How much oxygen does the human lung consume? *Anesthesiology* **86,** 532–537 (1997).
48. Wagner, D. E. *et al.* Comparative decellularization and recellularization of normal versus emphysematous human lungs. *Biomaterials* **35,** 3281–3297 (2014).
49. Hogan, B. L. *et al.* Repair and regeneration of the respiratory system: complexity, plasticity, and mechanisms of lung stem cell function. *Cell Stem Cell* **15,** 123–138 (2014).
50. Sachs, D. H. *et al.* Transplantation in miniature swine. I. Fixation of the major histocompatibility complex. *Transplantation* **22,** 559–567 (1976).
51. Voyta, J. C., Via, D. P., Butterfield, C. E. & Zetter, B. R. Identification and isolation of endothelial cells based on their increased uptake of acetylated-low density lipoprotein. *J. Cell Biol.* **99,** 2034–2040 (1984).
52. Islam, M. N., Gusarova, G. A., Monma, E., Das, S. R. & Bhattacharya, J. F-actin scaffold stabilizes lamellar bodies during surfactant secretion. *Am. J. Physiol. Lung Cell Mol. Physiol.* **306,** L50–L57 (2014).
53. Rampersad, S. N. Multiple applications of Alamar Blue as an indicator of metabolic function and cellular health in cell viability bioassays. *Sensors* **12,** 12347–12360 (2012).
54. Francis, R. & Lo, C. *Ex vivo* method for high resolution imaging of cilia motility in rodent airway epithelia. *J. Vis. Exp.* **78,** e50343 (2013).
55. Gibson-Corley, K. N., Olivier, A. K. & Meyerholz, D. K. Principles for valid histopathologic scoring in research. *Vet. Pathol.* **50,** 1007–1015 (2013).
56. Reece, T. B. *et al.* Adenosine A 2A receptor activation reduces inflammation and preserves pulmonary function in an *in vivo* model of lung transplantation. *J. Thorac. Cardiovasc. Surg.* **129,** 1137–1143 (2005).
57. Mulloy, D. P. *et al. Ex vivo* rehabilitation of non–heart-beating donor lungs in preclinical porcine model: delayed perfusion results in superior lung function. *J. Thorac. Cardiovasc. Surg.* **144,** 1208–1216 (2012).
58. Gimble, J. M., Katz, A. J. & Bunnell, B. A. Adipose-derived stem cells for regenerative medicine. *Circ. Res.* **100,** 1249–1260 (2007).
59. Huang, S. X. *et al.* Efficient generation of lung and airway epithelial cells from human pluripotent stem cells. *Nat. Biotechnol.* **32,** 84–91 (2014).

Acknowledgements

The authors thank J. Sonett and A. Griesemer for discussions of the experimental design; D. Sachs for providing research swine; S. Halligan for administrative and logistical support; the Institute of Comparative Medicine veterinary staff, including K. Fragoso and A. Rivas, for their support with the animal studies; S. Ma for live cell imaging; B. Lee and H. Wobma for manuscript review; K. Brown and L. Cohen-Gould for TEM imaging; the Herbert Irving Comprehensive Cancer Center Molecular Pathology Shared Resources, including T. Wu, D. Sun and R. Chen for help with the analytics; M. Cheerharan, M. P. Salna and A. Taubman for experimental assistance; V. Dorrello for valuable discussions; J. Bernhard and J. Ng for providing mesenchymal cells; J. Bhattacharya for providing experimental reagents. The authors gratefully acknowledge funding support from the National Institutes of Health (grants HL134760, EB002520 and HL007854), the Richard Bartlett Foundation and the Mikati Foundation.

Author contributions

J.D.O., B.A.G., J.K., S.C., D.Q., K.F., A.R. and M.B. performed the experiments. S.X.L.H. provided the human lung stem cells and experimental reagents. Y.-W.C. performed the live imaging. C.M. performed the blinded pathologic assessment. J.D.O., B.A.G., H.-W.S., M.B. and G.V.-N. co-analysed the data. J.D.O., B.A.G., H-W.S., M.B. and G.V.-N co-wrote the manuscript.

Additional information

Supplementary information is available for this paper.

Reprints and permissions information is available at www.nature.com/reprints.

Correspondence and requests for materials should be addressed to M.B. and G.V.-N.

How to cite this article: O'Neill, J. D. *et al.* Cross-circulation for extracorporeal support and recovery of the lung. *Nat. Biomed. Eng.* **1,** 0037 (2017).

Competing interests

The authors declare no competing financial interests.